





IP₇-SPX Domain Interaction Controls Fungal Virulence by Stabilizing Phosphate Signaling Machinery

Desmarini Desmarini,^{a,b,c}  Sophie Lev,^{a,b,c} David Furkert,^d Ben Crossett,^e Adolfo Saiardi,^f Keren Kaufman-Francis,^{a,b,c} Cecilia Li,^c Tania C. Sorrell,^{a,b,c} Lorna Wilkinson-White,^g Jacqueline Matthews,^g Dorothea Fiedler,^d  Julianne Teresa Djordjevic^{a,b,c}

^aCentre for Infectious Diseases and Microbiology, The Westmead Institute for Medical Research, Sydney, NSW, Australia

^bSydney Medical School-Westmead, University of Sydney, Sydney, NSW, Australia

^cMarie Bashir Institute for Infectious Diseases and Biosecurity, University of Sydney, Sydney, NSW, Australia

^dLeibniz-Forschungsinstitut für Molekulare Pharmakologie, Berlin, Germany

^eSydney Mass Spectrometry, University of Sydney, Sydney, NSW, Australia

^fMedical Research Council Laboratory for Molecular Cell Biology, University College London, London, United Kingdom

^gSchool of Life and Environmental Sciences, University of Sydney, Sydney, NSW, Australia

Desmarini Desmarini and Sophie Lev contributed equally to this article. Author order was determined alphabetically.

ABSTRACT In the human-pathogenic fungus *Cryptococcus neoformans*, the inositol polyphosphate signaling pathway is critical for virulence. We recently demonstrated the key role of the inositol pyrophosphate IP₇ (isomer 5-PP-IP₅) in driving fungal virulence; however, the mechanism of action remains elusive. Using genetic and biochemical approaches, and mouse infection models, we show that IP₇ synthesized by Kcs1 regulates fungal virulence by binding to a conserved lysine surface cluster in the SPX domain of Pho81. Pho81 is the cyclin-dependent kinase (CDK) inhibitor of the phosphate signaling (PHO) pathway. We also provide novel mechanistic insight into the role of IP₇ in PHO pathway regulation by demonstrating that IP₇ functions as an intermolecular “glue” to stabilize Pho81 association with Pho85/Pho80 and, hence, promote PHO pathway activation and phosphate acquisition. Blocking IP₇-Pho81 interaction using site-directed mutagenesis led to a dramatic loss of fungal virulence in a mouse infection model, and the effect was similar to that observed following *PHO81* gene deletion, highlighting the key importance of Pho81 in fungal virulence. Furthermore, our findings provide additional evidence of evolutionary divergence in PHO pathway regulation in fungi by demonstrating that IP₇ isomers have evolved different roles in PHO pathway control in *C. neoformans* and nonpathogenic yeast.

IMPORTANCE Invasive fungal diseases pose a serious threat to human health globally with >1.5 million deaths occurring annually, 180,000 of which are attributable to the AIDS-related pathogen, *Cryptococcus neoformans*. Here, we demonstrate that interaction of the inositol pyrophosphate, IP₇, with the CDK inhibitor protein, Pho81, is instrumental in promoting fungal virulence. IP₇-Pho81 interaction stabilizes Pho81 association with other CDK complex components to promote PHO pathway activation and phosphate acquisition. Our data demonstrating that blocking IP₇-Pho81 interaction or preventing Pho81 production leads to a dramatic loss in fungal virulence, coupled with Pho81 having no homologue in humans, highlights Pho81 function as a potential target for the development of urgently needed antifungal drugs.

KEYWORDS IP₇, inositol pyrophosphate, inositol polyphosphate, SPX domain, cyclin-dependent kinase inhibitor, PHO pathway, Pho81, *Cryptococcus neoformans*, fungal virulence

Citation Desmarini D, Lev S, Furkert D, Crossett B, Saiardi A, Kaufman-Francis K, Li C, Sorrell TC, Wilkinson-White L, Matthews J, Fiedler D, Djordjevic JT. 2020. IP₇-SPX domain interaction controls fungal virulence by stabilizing phosphate signaling machinery. *mBio* 11:e01920-20. <https://doi.org/10.1128/mBio.01920-20>.

Editor Xiaorong Lin, University of Georgia

Copyright © 2020 Desmarini et al. This is an open-access article distributed under the terms of the [Creative Commons Attribution 4.0 International license](https://creativecommons.org/licenses/by/4.0/).

Address correspondence to Julianne Teresa Djordjevic, julianne.djordjevic@sydney.edu.au.

Received 15 July 2020

Accepted 18 September 2020

Published 20 October 2020

Cryptococcus neoformans causes fatal meningitis worldwide, especially in immunosuppressed individuals and is responsible for more than 220,000 infections and 180,000 deaths annually (1). Infection is initiated in the lungs and can spread via the blood to the brain to cause meningitis that is fatal without treatment. All fungi, including *C. neoformans*, use signaling pathways to respond and adapt to host stress and hence to promote their pathogenicity (2). The inositol polyphosphate synthesis pathway, which produces the inositol pyrophosphate 5-PP-IP₅ (IP₇) (3–8), and the phosphate sensing and acquisition (PHO) pathway (3, 5) are essential for fungal growth in the lung and spread of infection to the brain. However, whether 5-PP-IP₅-mediated virulence impairment is due to defects in phosphate homeostasis remains to be addressed.

As an organism with a haploid genome, *C. neoformans* served as a useful model to pioneer the characterization of the inositol polyphosphate synthesis pathway in a human fungal pathogen (3–8). Using an inositol polyphosphate kinase (IPK) gene deletion approach to block IP production at different sites, it was shown that the inositol pyrophosphate, 5-PP-IP₅, is produced by the sequential phosphorylation of inositol trisphosphate (IP₃) by the IPKs Arg1, Ipk1, and Kcs1 and that 5-PP-IP₅ is the direct product of Kcs1 (Fig. 1A). In comparison to the other IP products in the pathway, loss of 5-PP-IP₅ had the most negative impact on virulence in a mouse model (4). 5-PP-IP₅ is the main IP₇ isomer in eukaryotic cells and consists of a *myo*-inositol backbone with five covalently attached phosphates and one di(pyro)phosphate at position 5. 5-PP-IP₅ is further phosphorylated at position 1 by Asp1 to produce 1,5-PP₂-IP₄ (IP₈) (9, 10). Loss of IP₈ had minimal impact on cellular function and virulence (4). The role of 5-PP-IP₅ in other human fungal pathogens has not been determined, presumably due to the inability to create viable IPK deletion mutants. However, the creation of a heterozygous *ARG1//IPK2* deletion mutant in *Candida albicans* demonstrated important roles for IPK products in cellular function (11).

Although 5-PP-IP₅ plays a critical role in fungal virulence, it is unclear how it functions at the molecular level. In nonpathogenic fungi, plants and mammalian cells inositol pyrophosphates, which are highly negatively charged, form electrostatic interactions with the positively charged binding pocket of SPX domains found in components of the phosphate homeostasis machinery (12–20). The term SPX is derived from the proteins in which the domain was first discovered (*Syg1*, *Pho81*, and *Xpr1*). SPX domains are small (135 to 380 residues long). They are either located at the N termini of proteins or occur as independent, single-domain proteins. The interaction of inositol polyphosphates with SPX domains has been shown to modulate phosphate sensing, transport and storage (16, 21).

In fungi, phosphate homeostasis is regulated by the PHO pathway. The mechanism of PHO pathway regulation in the model yeast, *Saccharomyces cerevisiae*, and in *C. neoformans* is mostly conserved, except for the absence of a transcriptional coregulator in *C. neoformans*, which coincides with an expanded number of gene targets (22, 23). In both organisms, phosphate deprivation is sensed by a core regulatory CDK complex comprised of the kinase Pho85, the cyclin Pho80, and the CDK inhibitor (CKI) Pho81, which initiates a transcriptional response aimed at restoring cellular phosphate levels (3, 5, 24, 25). When phosphate is abundant, Pho85 is active and phosphorylates the transcription factor Pho4, thus facilitating its export from the nucleus. When phosphate is scarce, Pho81 inhibits Pho85, preventing Pho4 phosphorylation and its export from the nucleus. This leads to the induction of genes involved in the acquisition of phosphate and potentially other nutrients in the case of *C. neoformans* (22, 26, 27). Blocking transcriptional activation of the PHO genes in *C. neoformans* and *C. albicans* by deleting the Pho4-encoding gene attenuated virulence in a mouse infection model (3, 28). In *S. cerevisiae*, activation of the PHO pathway requires the Vip1-derived IP₇ isomer, 1-PP-IP₅ (29).

In this study, we investigate the role of Kcs1-derived 5-PP-IP₅ in PHO pathway activation in the fungal pathogen *C. neoformans* and provide evidence of additional evolutionary divergence in PHO pathway regulation in fungi. We also show that the

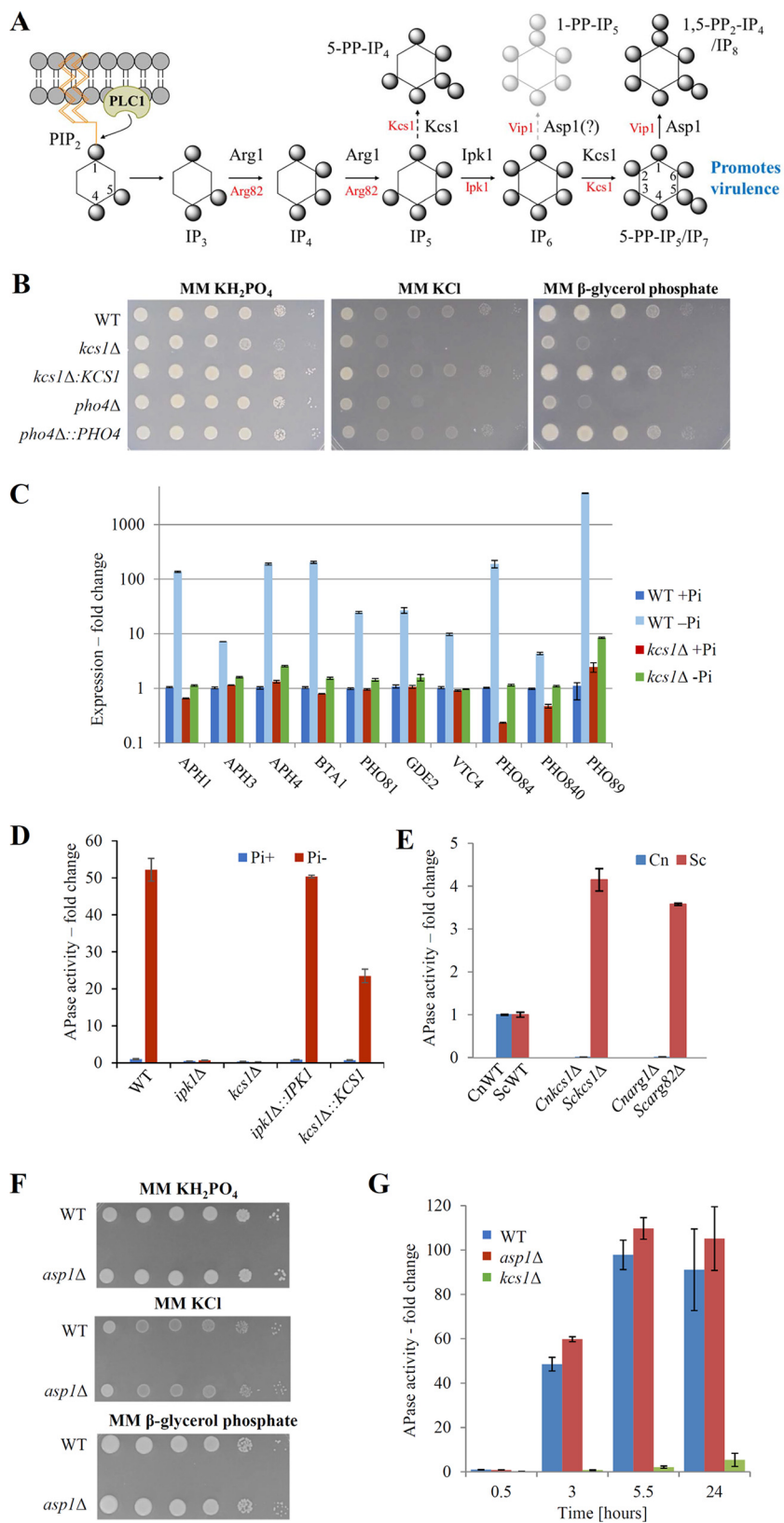


FIG 1 Kcs1-derived 5-PP-IP₅ is the only inositol polyphosphate required for PHO pathway activation in *C. neoformans* and has opposing roles in PHO pathway activation in *C. neoformans* and *S. cerevisiae*. (A) Inositol polyphosphate biosynthetic pathways in *C. neoformans* and *S. cerevisiae*. Spheres represent phosphate groups. Cryptococcal enzymes are indicated in black, and enzymes for *S. cerevisiae* are (Continued on next page)

critical roles of 5-PP-IP₅ and Pho81 in virulence are conveyed primarily via 5-PP-IP₅ interaction with the SPX domain of Pho81 and provide novel mechanistic insight into how inositol pyrophosphates regulate PHO pathway activation.

RESULTS

Kcs1-derived 5-PP-IP₅ is required for PHO pathway activation in *C. neoformans*.

The inositol polyphosphate biosynthetic pathway in *C. neoformans* is represented in Fig. 1A. 5-PP-IP₅, derived from Kcs1, is the major IP₇ isomer in fungi. Kcs1 activity is also necessary for the subsequent generation of 1,5-PP₂-IP₄ (IP₈) by Asp1. To determine whether these inositol pyrophosphates play a role in phosphate homeostasis in *C. neoformans*, growth of the *kcs1Δ* and *pho4Δ* strains was compared in the absence of free phosphate. The results in Fig. 1B demonstrate that growth of both strains is similarly attenuated in either phosphate-free medium (MM-KCl) or in medium where all phosphate is covalently bound to glycerol (β -glycerol-phosphate).

Next, we investigated whether delayed growth of the *kcs1Δ* mutant in the absence of phosphate correlates with an inability to upregulate genes involved in phosphate acquisition (PHO genes). PHO genes in *C. neoformans* encode three acid phosphatases, including secreted Aph1, which is a biochemical reporter for PHO pathway activation (5, 25); three high-affinity phosphate transporters (Pho84, Pho840, and Pho89) (24); Vtc4 (a component of the Vacuolar Transport Chaperone complex involved in synthesizing inorganic polyphosphate as a phosphate store) (12, 24); two proteins involved in lipid remodeling and phosphate conservation (betaine lipid synthase [Bta1] and glycerophosphodiesterase [Gde2]) (30, 31); and the CDKI, Pho81. Expression of these genes is upregulated in the wild type (WT) following phosphate starvation and is controlled by the transcription factor Pho4 (3, 4, 24, 25). Similar to the *pho4Δ* mutant (3), the PHO genes remained suppressed in the *kcs1Δ* mutant relative to the WT (Fig. 1C), indicating that 5-PP-IP₅ (the product of Kcs1) and/or its derivative 1,5-PP₂-IP₄ (produced by Asp1) are essential for PHO pathway activation and that the precursors of 5-PP-IP₅ (IP₃, IP₄, IP₅, and IP₆) play little or no role in the PHO pathway activation.

In a previous study, we showed that the cryptococcal *ipk1Δ* mutant accumulates significant quantities of another inositol pyrophosphate, 5-PP-IP₄. The *ipk1Δ* mutant is deficient in the native Kcs1 substrate IP₆. Consequently, Kcs1 phosphorylates IP₅ at the 5 position to form 5-PP-IP₄. Using the *ipk1Δ* mutant, we investigated whether 5-PP-IP₄, which has a similar structure to 5-PP-IP₅, can also promote PHO pathway activation. Production of extracellular acid phosphatase was used as a reporter to quantify PHO pathway activation in phosphate-starved WT and mutant cells. The results in Fig. 1D

FIG 1 Legend (Continued)

indicated in red. In *C. neoformans*, phospholipase C1 (PLC1)-derived IP₃ is sequentially phosphorylated to IP₄₋₅ and IP₆ by Arg1 and Ipk1, respectively. Kcs1 generates PP-IP₄ and 5-PP-IP₅/IP₇ from IP₅ and IP₆, respectively. However, PP-IP₄ is only detected in the *ipk1Δ* mutant. Asp1-derived 1,5-PP₂-IP₄, but not 1-PP-IP₅, has been detected in *C. neoformans*. (B) 5-PP-IP₅ is required for optimal growth in the absence of phosphate. Overnight YPD cultures were serially diluted (10⁶ to 10¹ cells per 5 μ l) and spotted onto YPD agar. Plates were incubated at 30 and 37°C for 2 days before being photographed. Growth of the 5-PP-IP₅-deficient *C. neoformans* mutant strain (*kcs1Δ*) is attenuated to a similar extent as the PHO pathway activation-defective mutant strain (*pho4Δ*). (C) Expression of phosphate-responsive genes regulated by Pho4 is compared by qPCR following growth in the presence and absence of phosphate (calculated using the $-\Delta\Delta C_T$ method and *ACT1* as the housekeeping gene). The expression in each strain is normalized to the WT +Pi. (D) 5-PP-IP₄ cannot substitute for 5-PP-IP₅ in promoting PHO pathway induction since the *ipk1Δ* mutant strain, which accumulates 5-PP-IP₄, fails to activate the PHO pathway in response to phosphate deprivation. APase activity refers to the extent of *p*-nitrophenyl phosphate hydrolysis by extracellular APases quantified spectrophotometrically at 420 nm (see Materials and Methods for a detailed description). The results are expressed as fold change relative to WT+Pi. (E) 5-PP-IP₅ has opposing roles in PHO pathway activation in *C. neoformans* (Cn) and *S. cerevisiae* (Sc). PHO pathway activation during phosphate deprivation is compared in WT Cn and Sc and their congenic 5-PP-IP₅-deficient strains (*arg1Δ/ipk2Δ* and *kcs1Δ*). APase activity was measured as in panel D and normalized to the APase activity of the corresponding WT strains. (F and G) Asp1-derived 1-PP-IP₅ and 1,5-PP₂-IP₄ are dispensable for PHO pathway activation and growth of *C. neoformans* during phosphate deprivation. A drop dilution test was performed as described previously (see panel B). In panel G, PHO pathway activation was assessed using the APase activity assay and normalized to WT at 0.5 h. All bar graphs represent the means \pm the standard deviations of three biological replicates.

demonstrate that, despite its structural similarity to 5-PP-IP₅ and high abundance in the *ipk1Δ* mutant strain, 5-PP-IP₄ cannot substitute for the native Kcs1 products in activating the PHO pathway, even though it alleviated some of the *kcs1Δ*-specific phenotypic defects (7).

In contrast to what we observed in *C. neoformans* (Fig. 1C and D), previous reports in *S. cerevisiae* suggest that PHO gene expression is constitutively active in the *kcs1Δ* mutant (32). To investigate this further, we assessed PHO pathway activation in WT *C. neoformans* and *S. cerevisiae* and their congenic 5-PP-IP₅-deficient mutant strains (*Cnarg1Δ/Scarg82Δ* and *kcs1Δ*) in parallel. The results in Fig. 1E confirm that the absence of Kcs1-derived inositol pyrophosphates does elicit opposite effects on PHO pathway activation in the two yeast species. Hyperactivation of the PHO pathway in the *Sckcs1Δ* mutant is consistent with that observed by Auesukaree et al. (32).

Asp1/Vip1-derived inositol pyrophosphates are dispensable for PHO pathway activation in *C. neoformans* and *S. cerevisiae*. Asp1 (*C. neoformans*) and its ortholog Vip1 (*S. cerevisiae*) phosphorylate 5-PP-IP₅ to produce 1,5-PP₂-IP₄ (4). Vip1 also phosphorylates IP₆ to produce an alternate isomer of IP₇, 1-PP-IP₅. Although we have never detected 1-PP-IP₅ in WT *C. neoformans* or in the *kcs1Δ* mutant (4), we considered the possibility that Asp1 produces small quantities of 1-PP-IP₅ in *C. neoformans*. To investigate the involvement of 1-PP-IP₅ and 1,5-PP₂-IP₄ in PHO pathway activation in *C. neoformans*, we employed the *ASP1* deletion mutant (*asp1Δ*). First, we assessed growth of *asp1Δ* on minimal medium (MM) without phosphate and in the presence of β-glycerol-phosphate as the only source of phosphate. Under both conditions, the growth of *asp1Δ* and WT strains was similar (Fig. 1F). This contrasted with the compromised growth observed for the *kcs1Δ* mutant. Next, we quantified PHO pathway activation in WT, *kcs1Δ*, and *asp1Δ* strains using the acid phosphatase reporter assay. Cultures were shifted from phosphate-replete to phosphate-deficient medium and production of secreted acid phosphatase was measured for up to 24 h. Similar to the results shown in Fig. 1C to E, acid phosphatase activity was almost abolished in the *kcs1Δ* mutant over the experimental time course (Fig. 1G). In contrast, acid phosphatase activity in WT and *asp1Δ* strains had increased ~100-fold by 5.5 h of phosphate deprivation and plateaued out to 24 h. Thus, Kcs1-derived 5-PP-IP₅, but neither 1-PP-IP₅ nor 1,5-PP₂-IP₄, promotes PHO pathway activation in *C. neoformans*. Vip1-derived IP₇ was implicated in PHO pathway activation in *S. cerevisiae* (29). However, we found phosphate deprivation-induced PHO pathway activation to be comparable in the *S. cerevisiae* WT and *vip1Δ* mutant (see Fig. S1 in the supplemental material). Overall, the results in Fig. 1 show that, in contrast to *S. cerevisiae*, Kcs1-derived 5-PP-IP₅ is the main IPK pathway product involved in PHO pathway activation in *C. neoformans* and suggest that the PHO pathway has become rewired in *C. neoformans*.

5-PP-IP₅ acts upstream of CDK Pho85 to promote PHO pathway activation. During phosphate deprivation, the CKI Pho81 blocks Pho85 kinase activity and hence phosphorylation of the transcription factor Pho4. Pho4 is subsequently retained in the nucleus to induce expression of PHO genes. In humans, yeast, and plants, inositol pyrophosphates interact with the SPX domain of proteins, including the SPX domain of Pho81 in *S. cerevisiae* (12–14, 16–18, 20, 33, 34). Like ScPho81, Pho81 in *C. neoformans* also has an SPX domain. We therefore hypothesized that 5-PP-IP₅ interacts with cryptococcal Pho81 to modulate PHO pathway activation.

As a first step to testing this hypothesis, we used the CDK inhibitor Purvalanol A to bypass Pho81 inhibition (3, 35) and assess whether the PHO pathway can be reactivated in the absence of 5-PP-IP₅. The results show that even when phosphate is present, Purvalanol A derepresses the PHO pathway in the WT and 5-PP-IP₅-deficient mutants, including the *kcs1Δ* mutant, but not in the *pho4Δ* control strain, in which PHO pathway activation is blocked downstream of Pho85 (see Fig. S2A and B). Furthermore, we observed a progressive derepression of the PHO pathway up to 50 μM Purvalanol A in WT and *kcs1Δ* strains irrespective of phosphate status with the effect plateauing at 50 μM (see Fig. S2C). These data suggest that 5-PP-IP₅ functions upstream of Pho85 to inhibit Pho85 kinase activity and promote PHO pathway activation.

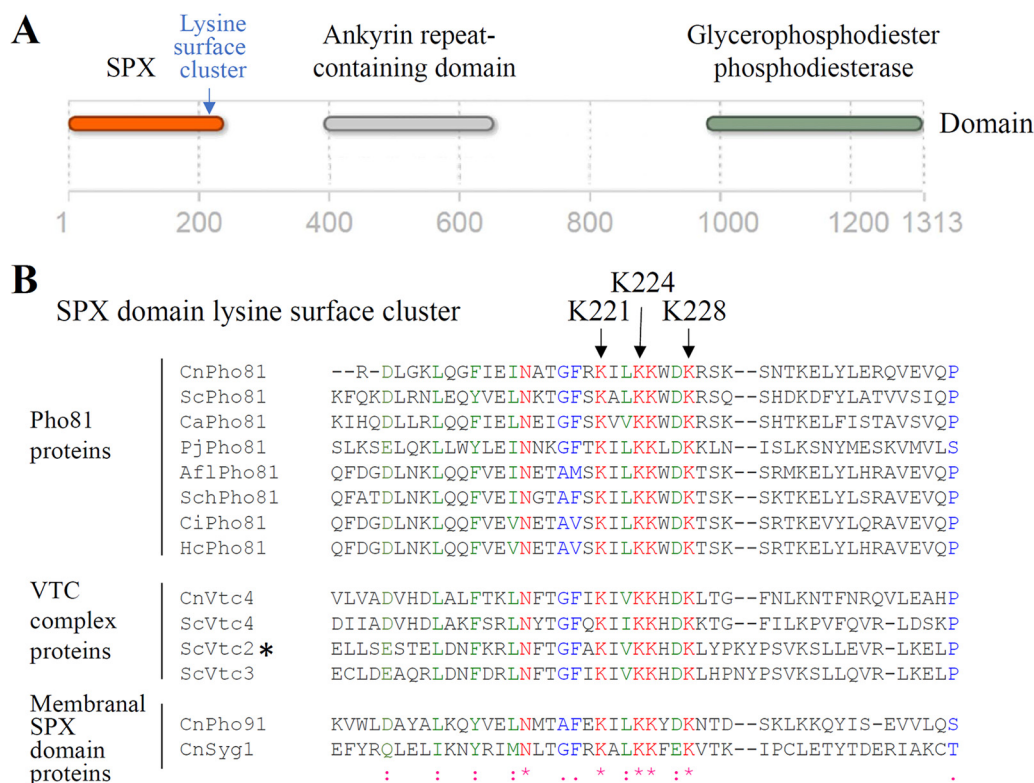


FIG 2 Key IP₇-binding residues in SPX domains are conserved in Pho81 homologs from numerous virulent fungi. (A) Fungal Pho81 homologues (cryptococcal Pho81 shown as a representative) contain an SPX domain with a lysine surface cluster, an ankyrin repeat domain, and a glycerophosphodiester phosphodiesterase (GDE) domain. (B) Alignment of the SPX domain lysine surface cluster region of CnPho81 and other fungal proteins. A role for the lysine surface cluster in inositol polyphosphate binding has been validated in ScVtc2 (*). Proteins used in the alignment: *Cryptococcus neoformans* var. *grubii* H99 CnPho81 (XP_012049680), CnSyl1 (XP_012051471), CnPho91 (XP_012049822) phosphate transporter, and CnVtc4 (XP_012049426) vacuolar transporter chaperone 4; *Saccharomyces cerevisiae* ScPho81 (SGDID:S000003465), ScVtc4 (SGDID:S000003549), ScVtc2 (SGDID:S000001890), and ScVtc3 (SGDID:S000005940); *Histoplasma capsulatum* HcPho81 (EHH08674); *Pneumocystis jirovecii* PjPho81 (XP_018228495); *Candida albicans* CaPho81 (XP_718633); *Stachybotrys chartarum* SchPho81 (KFA80477); *Aspergillus flavus* AflPho81 (RAQ58413); and *Coccidioides immitis* CiPho81 (XP_001244784).

Key IP₇-binding residues in SPX domains are conserved in Pho81 homologs from numerous virulent fungi.

Pho81 homologs from numerous fungal species, including *C. neoformans* and others known to infect humans, contain an N-terminal SPX domain with a lysine surface cluster putatively involved in binding inositol pyrophosphates (Fig. 2A). The SPX domain is followed by an ankyrin repeat domain and a glycerophosphodiester phosphodiesterase domain. The GDE domain in cryptococcal (Cn) Pho81 does not contain critical catalytic residues involved in phospholipid hydrolysis and hence is most likely enzymatically inactive. Alignment of the CnPho81 SPX domain with SPX domains from other fungal proteins, including ScVtc2 for which a role for the basic surface cluster in inositol polyphosphate binding has been validated by site-directed mutagenesis (16), demonstrated the conservation of key lysine residues in CnPho81 (Fig. 2B). We adopted the strategy used by Wild et al. (16) to alter K^{221,224,228} in the cryptococcal Pho81 SPX domain to alanine, creating the Pho81SPX^{AAA} strain to assess the contribution of 5-PP-IP₅-Pho81 interaction to Pho81 function. The Pho81SPX control strain was taken through the same procedure as Pho81SPX^{AAA} and is therefore genetically identical except for the AAA mutation. As a control, we also deleted the entire *PHO81* gene (*pho81Δ*) (Table 1; see also Table S1, Fig. S3, and Fig. S4).

5-PP-IP₅ binding to the Pho81 SPX domain promotes PHO pathway activation.

To investigate the role of 5-PP-IP₅-Pho81 interaction in phosphate homeostasis, growth of the Pho81SPX^{AAA} strain was compared to that of the WT and Pho81SPX control strains in the presence and absence of phosphate (Fig. 3A and B). The *pho81Δ* strain, its

TABLE 1 Strains used in this study

Strain	Genotype	Source or reference	Gene identification
<i>C. neoformans</i>			
<i>pho81Δ</i>	<i>pho81Δ::HYG</i>	This study	CNAG_02541
<i>Δpho81 + PHO81</i>	<i>pho81Δ::HYG PHO81-NEO</i>	This study	CNAG_02541
<i>spxΔ</i>	<i>spxΔ::HYG</i>	This study	Part of CNAG_02541
Pho81 ^{SPX}	<i>spxΔ::HYG NEO-GDE2p-SPX</i>	This study	CNAG_02541
Pho81 ^{SPXAAA}	<i>spxΔ::HYG NEO-GDE2p-SPX^{AAA}</i>	This study	CNAG_02541
GFP-Pho81	<i>spxΔ::HYG NEO-GDE2p-SPX PHO81-GFP-NAT</i>	This study	CNAG_02541
GFP-Pho81 ^{SPXAAA}	<i>spxΔ::HYG NEO-GDE2p-SPX^{AAA} PHO81-GFP-NAT</i>	This study	CNAG_02541
GFP-Pho81	<i>PHO81-GFP-NAT</i>	This study	CNAG_02541
GFP-Pho81 <i>kcs1Δ</i>	<i>kcs1Δ::NEO PHO81-GFP-NAT</i>	This study	CNAG_02541/CNAG_02897
<i>pcl6/7Δ^a</i>	<i>pcl6/7Δ::NAT</i>	MKL ^a	CNAG_05524
<i>arg1Δ</i>	<i>arg1Δ::NEO</i>	8	CNAG_06500
<i>kcs1Δ</i>	<i>kcs1Δ::NEO</i>	4	CNAG_02897
<i>kcs1Δ + KCS1</i>	<i>kcs1Δ::NEO KCS1-NAT</i>	4	CNAG_02897
<i>ipk1Δ</i>	<i>ipk1Δ::NEO</i>	7	CNAG_01294
<i>ipk1Δ + IPK1</i>	<i>ipk1Δ::NEO IPK1-HYG</i>	7	CNAG_01294
<i>asp1Δ</i>	<i>asp1Δ::NEO</i>	4	CNAG_02161
<i>pho4Δ</i>	<i>pho4Δ::NAT</i>	55	CNAG_06751
<i>pho4Δ::PHO4</i>	<i>pho4Δ::NAT PHO4 + NEO</i>	3	CNAG_06751
<i>S. cerevisiae</i>			
Wild type	<i>MATa his31 leu20 met150 ura30</i> (S288C)	ATCC	BY4741
<i>arg82Δ</i>	<i>arg82Δ</i>	ATCC	YDR173C
<i>kcs1Δ</i>	<i>MATa/MATα his3Δ1/his3Δ1 leu2Δ0/leu2Δ0 lys2Δ0/met15Δ0/ura3Δ0/ura3Δ0 kcs1Δ</i>	ATCC	YDR017C
<i>vip1Δ</i>	<i>MATa/MATα his3Δ1/his3Δ1 leu2Δ0/leu2Δ0 lys2Δ0/+ met15Δ0/+ ura3Δ0/ura3Δ0 ylr410w::KanMX4</i>	ATCC	YLR410W

^aMKL, Madhani knockout library (<http://www.fgsc.net/crypto/crypto.htm>) (2015).

reconstituted strain *pho81Δ + PHO81*, and the *pho4Δ* and *kcs1Δ* strains were included as controls. All strains had a similar growth rate in the presence of phosphate (Fig. 3A). In contrast, the growth rate of the Pho81SPX^{AAA} and *pho81Δ* mutant strains was reduced relative to that of the WT and Pho81SPX control strains in phosphate-deficient medium (Fig. 3B). As expected, growth of *kcs1Δ* and *pho4Δ* was also reduced in phosphate-deficient medium (Fig. 3B). Next, the role of 5-PP-IP₅-Pho81 interaction in PHO pathway activation was assessed using an acid phosphatase reporter assay (Fig. 3C). Similar to the growth assays, the PHO pathway activation was abrogated during phosphate deprivation in the Pho81SPX^{AAA}, *pho81Δ*, *kcs1Δ*, and *pho4Δ* mutant strains relative to that of the WT and Pho81SPX control strains. 5-PP-IP₅ levels have been reported to decline in *S. cerevisiae* in response to phosphate deprivation (16, 36). We now demonstrate that the same occurs in *C. neoformans* with a decline of approximately ~50% observed (Fig. 3D). Despite this decline, 5-PP-IP₅ levels are sufficient to promote PHO pathway activation in WT and Pho81SPX control strains.

We also confirmed that Pho81 associates with 5-PP-IP₅ via K^{221,224,228} in the SPX domain by performing affinity capture experiments using a 5-PP-IP₅-conjugated resin. To enable Pho81 detection by Western blotting, we added a green fluorescent protein (GFP) tag at the C terminus of WT and mutant Pho81 (see Fig. S3) and confirmed that tag addition did not affect functionality (see Fig. S5). The Pho81-GFP expressing strains were cultured in phosphate (P_i)-deficient and P_i-replete medium. Cell lysates were incubated with chemically synthesized affinity capture resins, presenting either a stable nonhydrolyzable version of 5-PP-IP₅ (5-PCP-IP₅) (37) or P_i (as a control), to pull down Pho81SPX-GFP and Pho81SPX^{AAA}-GFP. The extent of binding of native and mutant Pho81 proteins (molecular mass, 170.2 kDa) to each resin was compared by anti-GFP Western blotting (Fig. 4). Levels of Pho81SPX and Pho81SPX^{AAA} were more comparable in P_i-grown versus P_i-starved cells. Given that the protein concentration was similar in all lysates, increased Pho81SPX relative to Pho81SPX^{AAA} in P_i-starved cells is attributable to *PHO81* being a phosphate-responsive gene and the PHO pathway being functional only in the Pho81SPX strain (Fig. 1B). Hence, Pho81-mediated inhibition of

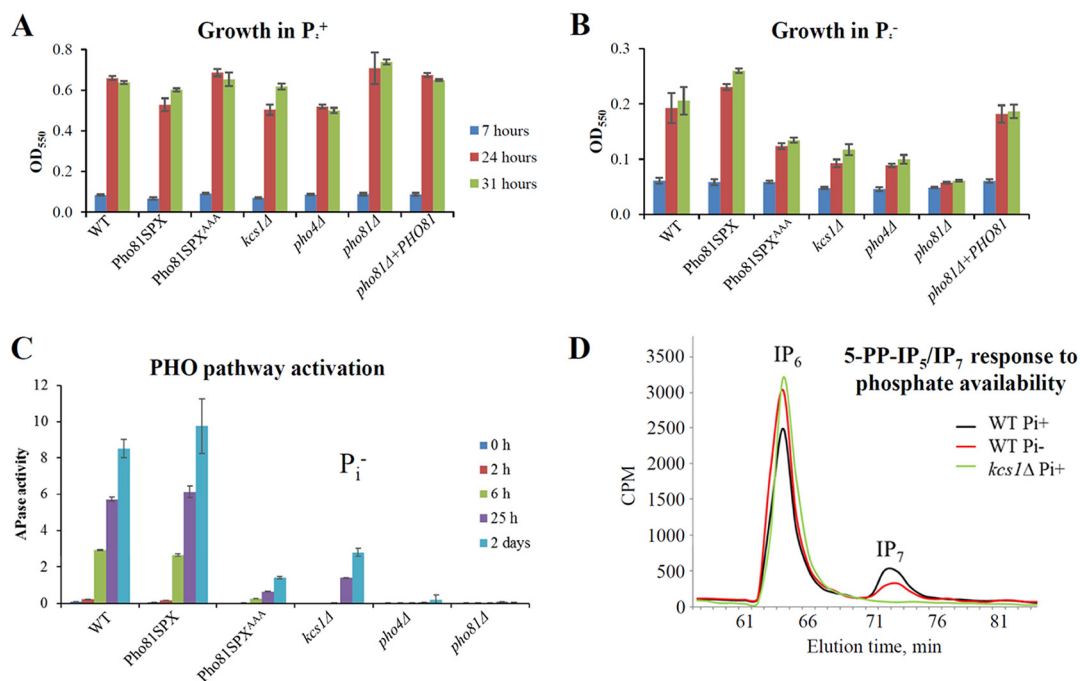


FIG 3 The lysine surface cluster in the Pho81 SPX domain is required for PHO pathway activation. The Pho81SPX^{AAA} and *pho81Δ* strains grow at a rate similar to that of WT, Pho81SPX, and *pho81Δ*+PHO81 strains in the presence (A), but not in the absence (B), of phosphate. In the absence of phosphate, the growth of the Pho81SPX^{AAA} strain is reduced to a level similar to that observed for the *pho81Δ*, *kcs1Δ*, and *pho4Δ* mutant strains. The strains were cultured for 7, 24, and 31 h in MM-KCl, and growth at each time point was assessed by measuring the optical density (550 nm) of the culture using a spectrophotometer. (C) The strains were cultured in MM-KCl, and the PHO pathway activation was assessed at the indicated times using the APase activity assay. APase activity refers to the extent of *p*-nitrophenyl phosphate hydrolysis by extracellular APases quantified spectrophotometrically at 420 nm. In panels A, B, and C, the results represent the means \pm the standard deviations of three biological replicates. (D) Comparison of the level of ³H-inositol-labeled 5-PP-IP₅ (IP₇) in the WT strain by anion-exchange HPLC following growth in P_i⁺ or P_i⁻ medium. The metabolic profile of the *kcs1Δ* strain following growth in YPD medium is provided to indicate the position of IP₇.

Pho85 drives its own induction during P_i starvation. The affinity capture results demonstrate that under both growth conditions, native Pho81 binds to the 5-PCP-IP₅, but not to the P_i resin. In contrast, the mutated variant does not bind to either resin but appears in the flowthrough. Thus, native Pho81SPX protein, but not its Pho81SPX^{AAA} variant, binds 5-PP-IP₅.

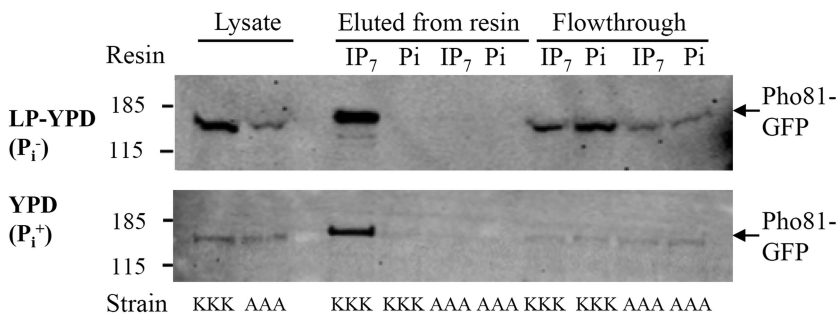


FIG 4 5-PP-IP₅ interacts with the Pho81 SPX domain via the lysine surface cluster. The GFP-labeled strains were cultured for 5 h in phosphate-depleted medium (LP-YPD) to induce PHO pathway activation or in phosphate-replete (YPD) medium as indicated. Cell pellets were lysed, and the total protein was adjusted to 8 mg/ml to correct for growth differences. Lysates were incubated with 5-PCP-IP₅-conjugated (IP₇) and phosphate (P_i)-conjugated (control) resin. Bound Pho81 from each strain was then compared by SDS-PAGE and anti-GFP Western blotting. Then, 10- μ l portions of protein-adjusted lysates prepared from Pho81SPX-GFP (KKK) and Pho81SPX^{AAA}-GFP (AAA), respectively, were run as controls. Adjacent lanes (from left to right) contain what was eluted from each resin by the LDS loading buffer and what was present in the flowthrough.

TABLE 2 CDK components consistently detected in the Pho81SPX-GFP and Pho85-mCherry immunoprecipitations regardless of phosphate status^a

Accession no.	GFP-labeled Pho81						mCherry-labeled Pho85					
	Pi depleted			Pi replete			Pi depleted			Pi replete		
	PEP	% Cov	PSMs	PEP	% Cov	PSMs	PEP	% Cov	PSMs	PEP	% Cov	PSMs
CNAG_01922 (Pho80)	74.52	43.42	46	55.16	33.33	55	87.03	38.16	46	99.93	43.42	50
CNAG_02541 (Pho81)	379.78	40.67	540	331.41	34.50	520	609.66	53.08	347	487.34	37.09	278
CNAG_08022 (Pho85)	138.83	47.32	137	104.12	35.20	143	188.63	51.52	147	176.39	37.76	152
CNAG_05524 (Pcl6)	152.28	62.39	112	83.81	37.97	29	181.42	65.10	113	210.59	55.70	99

^aAnti-GFP-Pho81 or anti-mCherry-Pho81 immunoprecipitations were separated by SDS-PAGE and the associated CDK components were identified by 1D-LC-MS. All CDK components (Pho81, Pho85, and Pho80) and an additional cyclin (Pcl6) were detected consistently in both sets of immunoprecipitations prepared from cells grown in phosphate-replete and phosphate-depleted medium. Control immunoprecipitations were also performed on the WT (no GFP or mCherry) and the absence of all CDK components was confirmed. The PEP score (PEP) is based on the probability of identification: scores above 3 are equivalent to a q-value of <0.002. “% Cov” is the percent coverage of the open reading frame the observed peptides match, while the number of peptide spectral matches (PSMs) is proportional to the protein abundance. All PSMs were filtered to ensure a <1% false discovery rate.

In *S. cerevisiae*, Pho81 forms a stable complex with Pho85-Pho80 independently of phosphate status, but only inhibits the CDK during phosphate deprivation (38). Interaction of Pho81 with Pho85-Pho80 is primarily via Pho80 (38, 39). To determine whether the association of CDK components in *C. neoformans* is phosphate dependent, the WT strains expressing either Pho81-GFP (see Fig. S3) or Pho85-mCherry were cultured in P_i-depleted and P_i-replete media. GFP trap and an anti-mCherry antibody were used to immunoprecipitate Pho81 and Pho85, respectively, and any associated proteins from cell lysates. CDK components were separated by SDS-PAGE and identified by one-dimensional liquid chromatography-mass spectrometry (1D-LC-MS). In both sets of immunoprecipitations, Pho81, Pho85, Pho80 and a second cyclin, glycogen storage control protein (CNAG_05524), were consistently detected in the CDK complex regardless of phosphate availability (Table 2). A BLAST search against the *S. cerevisiae* genome database using the glycogen storage control protein sequence as a query revealed that this cyclin is most similar to cyclins Pcl6 and Pcl7 which, among other cyclins, are most closely related to Pho80 (see Fig. S6A). Thus, we renamed this cyclin CnPcl6/7.

Of all the genes encoding CDK complex components, *PHO81* was the most phosphate responsive (~14-fold induction) (Fig. 1C; see also Fig. S6B), followed by *PHO80* and *PLC6/7* (~4- to ~5-fold induction) (see Fig. S6B). A small increase in *PHO85* gene expression (~1.8-fold) was observed but was not statistically significant. Although *PCL6/7* is phosphate-responsive, it is dispensable for PHO pathway activation as assessed using a *pcl6/7Δ* mutant (see Fig. S6B). Given its similarity to cyclin homologues involved in glycogen storage in *S. cerevisiae*, we investigated whether cryptococcal Pcl6/7 also has a role in glycogen storage. The results in Fig. S8 demonstrate reduced glucose induction of the glycogen metabolic genes, *GSY2/CNAG_04621* and *GLC3/CNAG_00393*, in the *pcl6/7Δ*, Pho81SPX^{AAA}, and *pho81Δ* strains relative to the WT. The results suggest that, in addition to activating the PHO pathway by interacting with Pho80-Pho85, 5-PP-IP₅-Pho81 modulates glycogen storage by interacting with Pcl6/7-Pho85.

PP-IP₅-Pho81 interaction stabilizes the CDK complex of the PHO pathway. To investigate whether 5-PP-IP₅ interaction with Pho81 affects Pho81 association with the CDK complex, Pho81SPX-GFP and Pho81SPX^{AAA}-GFP were immunoprecipitated from cells cultured in the presence and absence of P_i. Pho81-associated Pho85 was then quantified by Western blotting (Fig. 5A). Cdc2 in cell lysates was used as an indicator of sample protein concentration prior to immunoprecipitation. Under P_i-depleted conditions, Pho81SPX and Pho85 abundance increased to a similar extent (~2-fold) compared to their levels in cultures supplied with P_i (Fig. 5A, compare lanes 1 and 3), consistent with increased CDK complex formation. Increased Pho85 and Pho81 abundance following P_i deprivation correlated with increased *PHO85* and *PHO81* gene expression (see Fig. S6B: ~1.8-fold for *PHO85* and ~14-fold for *PHO81*). However, the

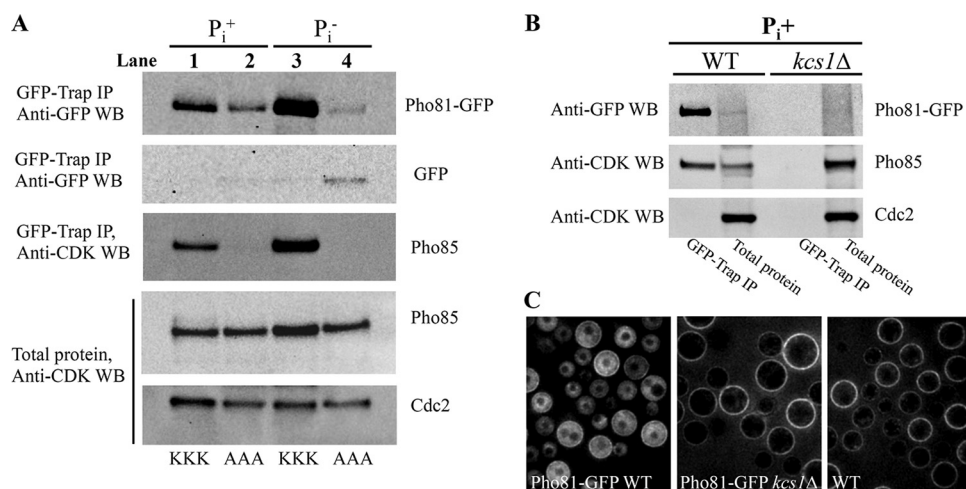


FIG 5 5-PP-IP₅-Pho81 interaction stabilizes the CDK complex of the PHO pathway. (A) GFP-trap was used to immunoprecipitate Pho81SPX-GFP (KKK, lanes 1 and 3) and Pho81SPX^{AAA}-GFP (AAA, lanes 2 and 4) from lysates following cell growth in P_i^+ and P_i^- medium. Immunoprecipitates and total cell lysates (control) were resolved by SDS-PAGE. Immunoprecipitated Pho81-GFP was detected by anti-GFP Western blotting. Anti-CDK antibody, which detects the PSTAIR motif, was used to detect Pho85 in the immunoprecipitates and cell lysates, as well as Cdc2 in the cell lysate, as indicated. The blot is representative of three biological replicates where, on average, Pho85/Pho81SPX^{AAA} association was 2.7-fold weaker than Pho85/Pho81SPX association in P_i^+ cultures. (B) GFP-trap was used to immunoprecipitate Pho81SPX-GFP from WT and *kcs1Δ* lysates following cell growth in P_i^+ medium. Immunoprecipitates and total cell lysates (control) were resolved by SDS-PAGE. Pho81-GFP, Pho85, and Cdc2 were detected by Western blotting as in panel A. (C) Pho81SPX-GFP is not detected by fluorescence microscopy (DeltaVision) in an IP₅-deficient (*kcs1Δ*) background following cell growth in P_i^+ medium (using the same conditions as in panel B). Autofluorescence of the cell walls is detected in all samples due to the prolonged exposure essential for observing Pho81-GFP.

increase in *PHO81* expression far exceeded the increase in Pho81 protein in the immunoprecipitates, consistent with translation of only a proportion of *PHO81* transcripts and/or rapid degradation of excess free Pho81.

Quantification of Pho85 association with native and mutant Pho81 in the absence of PHO pathway activation (P_i^+ culture) demonstrated weaker Pho85 binding to mutant Pho81 (Fig. 5A, compare lanes 1 and 2), suggesting that 5-PP-IP₅ is required for stabilizing the CDK complex. Interestingly, we observed that the abundance of Pho81SPX^{AAA} declined during P_i deprivation/PHO pathway activation (Fig. 5A, compare lanes 2 and 4), rendering comparison of Pho85 association with WT and mutant Pho81 during P_i deprivation unfeasible. Using qPCR, we ruled out reduction of *PHO81SPX^{AAA}* gene expression under inducing conditions as a possible explanation (see Fig. S8). Rather, the detection of cleaved GFP in the mutant sample (Fig. 5A, lane 4) was indicative of Pho81 degradation during P_i deprivation. The reduced stability of mutant Pho81 under these conditions coincides with lower levels of IP₇ (Fig. 3D).

To further investigate the impact of 5-PP-IP₅ interaction with Pho81 on CDK association, we tagged Pho81SPX with GFP in the *kcs1Δ* mutant background and repeated the immunoprecipitations on P_i^+ cultures. Pho81SPX protein was not detected in *kcs1Δ* lysates (total protein) and immunoprecipitations (GFP-Trap IP) (Fig. 5B) or in intact 5-PP-IP₅-deficient cells by fluorescence microscopy (Fig. 5C). Once again, qPCR ruled out reduced *PHO81* gene expression as a possible explanation (Fig. 1C; see also Fig. S8, using GFP strains and growth conditions identical to those in Fig. 5B). Hence the results are consistent with degradation of Pho81, but not Pho85, in a 5-PP-IP₅-deficient environment.

From the results in Fig. 4 and 5, we propose a model (Fig. 6) where Pho81 stability and association with Pho85-Pho80 and Pho85-Pcl6/7 depends on its ability to bind 5-PP-IP₅ and where 5-PP-IP₅-Pho81 interaction promotes PHO pathway activation and glycogen biosynthesis.

5-PP-IP₅-Pho81 interaction is critical for fungal virulence and dissemination. To determine the impact of 5-PP-IP₅-Pho81 interaction on cryptococcal virulence, we

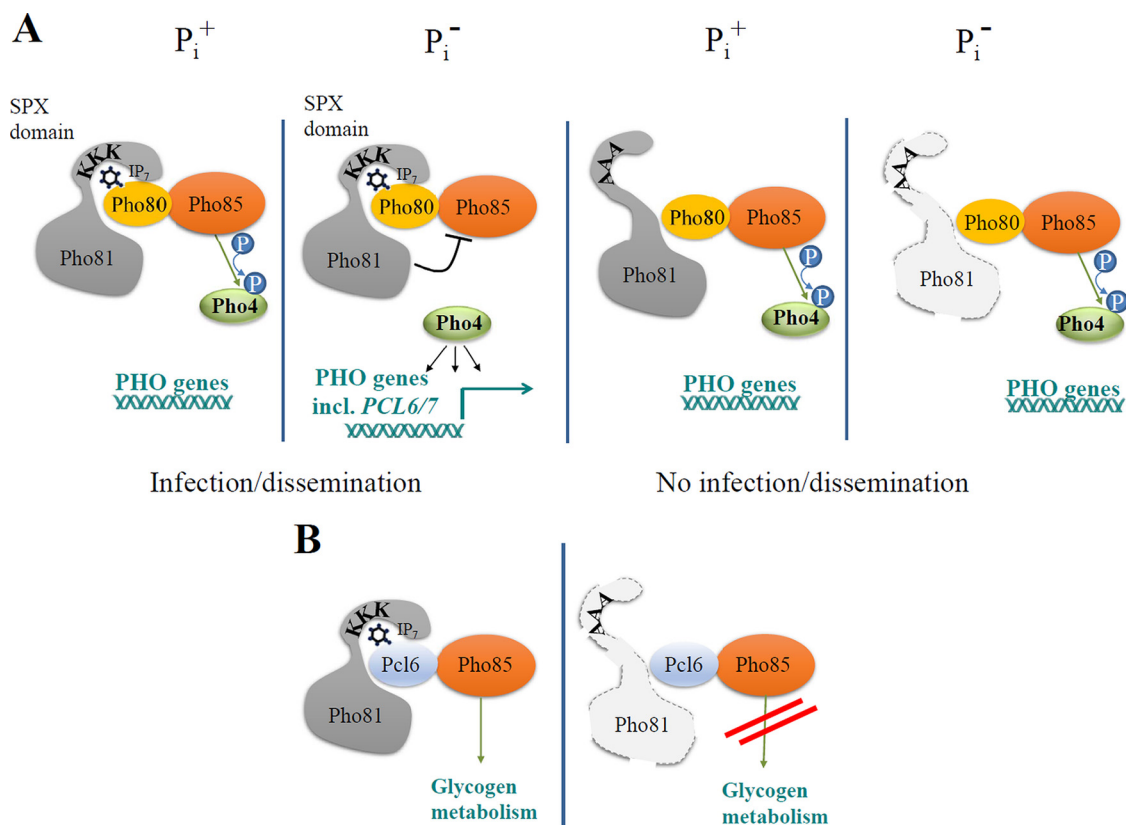
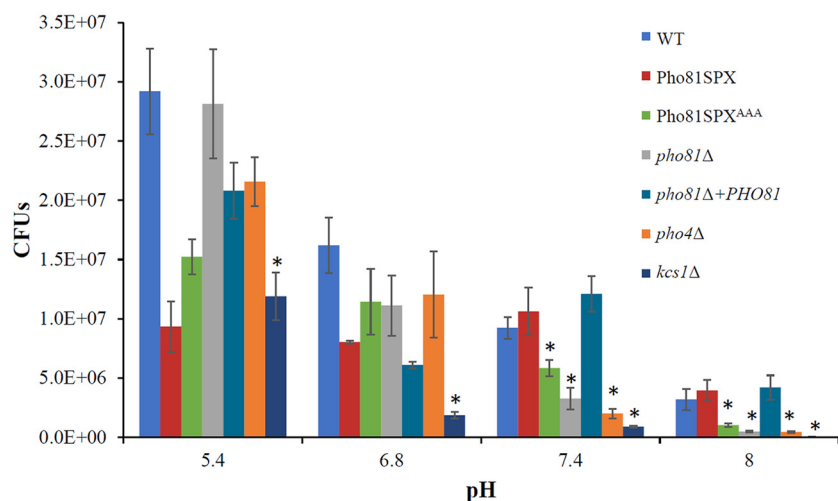


FIG 6 Model depicting the role of 5-PP-IP₅ in CDK stability and PHO pathway activation in *C. neoformans*. The binding of 5-PP-IP₅ to the SPX domain of Pho81 in *C. neoformans* promotes Pho81 association with Pho80-Pho85 (A) and Pcl6/7-Pho85 (B). 5-PP-IP₅, which is negatively charged, forms electrostatic interactions with the lysine surface cluster in the SPX domain of native Pho81 and with unidentified basic residues in cyclins Pho80 and Pcl6/7 and therefore stabilizes each CDK complex irrespective of phosphate status. In panel A, 5-PP-IP₅-bound Pho81 inhibits Pho85 during phosphate deprivation, preventing phosphorylation of Pho4 and triggering PHO pathway activation to promote pathogenicity. In contrast, 5-PP-IP₅ binding-defective Pho81 cannot form a stable complex with Pho80-Pho85 and Pho85 remains active, phosphorylating Pho4 to prevent PHO pathway activation. In panel B, 5-PP-IP₅-bound Pho81 may also regulate Pcl6-Pho85 to fine-tune glycogen metabolism. In both panels A and B, 5-PP-IP₅ binding-defective Pho81 is unstable and becomes degraded.

investigated whether the PHO pathway activation-defective Pho81SPX^{AAA} and *pho81Δ* mutant strains retained key virulence traits characteristic of *C. neoformans* (e.g., ability to grow at 37°C and produce capsule and melanin). We found that all phenotypes were identical to that of the Pho81SPX, WT, and *pho81Δ*+PHO81 strains (results not shown).

Despite the availability of significant levels of free phosphate in most environments within the mammalian host, the alkaline pH of host blood and tissues mimics phosphate starvation, leading to activation of the fungal PHO pathway (3, 40, 41). Consistent with this, the PHO pathway activation-defective cryptococcal strain, *pho4Δ*, exhibits reduced growth at alkaline (including host) pH, even when phosphate is available (3). We therefore compared growth of the PHO pathway activation defective Pho81SPX^{AAA} strain and the Pho81SPX control strain at acidic and basic pH and included the WT, *pho4Δ*, *kcs1Δ*, *pho81Δ*, and *pho81Δ*+PHO81 strains as additional controls (Fig. 7). At pH 5.4 and pH 6.8, none of the pairwise growth differences relative to the parent strain were statistically significant except for the WT versus the *kcs1Δ* strain. The reduced growth of *kcs1Δ* is expected since this mutant grows slower than the WT under nonstress conditions (YPD medium) due to Kcs1 having a pleiotropic role in cellular function (4). In contrast, at pH 7.4 and pH 8 (P_i^+), growth of the *pho4Δ*, *pho81Δ*, *kcs1Δ*, and Pho81SPX^{AAA} strains was reduced relative to the WT, Pho81SPX, and *pho81Δ*+PHO81 strains (Fig. 7) consistent with the alkaline pH environment mimicking phosphate deprivation (3, 40).



Dunnett's <i>post-hoc</i> test comparisons	5.4	6.8	7.4	8
H99 WT vs. <i>pho4Δ</i>	0.1758	0.5635	0.0043	0.0005
H99 WT vs. <i>pho81Δ</i>	0.9994	0.2395	0.0058	0.0005
H99 WT vs. <i>pho81Δ+PHO81</i>	0.1526	0.0531	0.2272	0.2447
H99 WT vs. Pho81SPX	0.0144	0.0787	0.8350	0.4996
H99 WT vs. Pho81SPX ^{AAA}	0.0315	0.3089	0.0303	0.0035
H99 WT vs. <i>kcs1Δ</i>	0.0203	0.0268	0.0125	0.0001
Pho81SPX vs. Pho81SPX ^{AAA}	0.0709	0.2775	0.0007	0.0003

FIG 7 5-PP-IP₅-Pho81 interaction is required for fungal growth at alkaline pH. The strains indicated were cultured in minimal media containing 1 mM KH₂PO₄ with the pH adjusted to 6.8, 7.4, or 8.0 with HEPES buffer and to pH 5.4 with MES buffer. Growth was assessed after 24 h with shaking by quantitative culture (CFU). Results represent the means ± the standard deviations of three biological replicates. Statistical analysis was performed using one-way ANOVA. With the exception of *kcs1Δ**, none of the Dunnett's *post hoc* test comparisons at pH 5.4 and 6.8 were statistically significant relative to their control strain ($P \geq 0.05$). However, at pH 7.4 and pH 8, growth of the *pho4Δ*, *pho81Δ*, *kcs1Δ*, and Pho81SPX^{AAA} strains was reduced relative to the WT, Pho81SPX, and *pho81Δ+PHO81* strains (*, $P < 0.05$), consistent with the alkaline pH environment mimicking phosphate deprivation.

Next, we assessed what effect blocking 5-PP-IP₅-Pho81 interaction had on fungal virulence in a mouse inhalation model, which mimics the natural route of infection in humans. All mice infected with the Pho81SPX control strain succumbed to infection with the median survival time being 23 days (Fig. 8A). In contrast, no mice infected with the Pho81SPX^{AAA} mutant became ill, and by 60 days postinfection their average weight had increased by $20 \pm 5.5\%$ relative to their average preinfection weight. Organ burdens determined in Pho81SPX-infected mice at time-of-death and in Pho81SPX^{AAA}-infected mice at 60 days postinfection show almost no infection in the lungs and brain of Pho81SPX^{AAA}-infected mice by 60 days postinfection (Fig. 8B and C). This is consistent with the inability of this strain to establish a lung infection and disseminate to the brain.

We also investigated the effect of deleting the *PHO81* gene on fungal virulence and included the *pho81Δ+PHO81* strain as a control (Fig. 8). For the survival analysis, the *pho81Δ* mutant strain behaved similarly to the Pho81SPX^{AAA} strain, with no *pho81Δ*-infected mice succumbing to infection over the 60-day time course (Fig. 8D). Furthermore, the *pho81Δ*-infected mice had gained a similar amount of weight by 60 days postinfection as the Pho81SPX^{AAA}-infected mice. As expected, *pho81Δ+PHO81*-infected mice had a similar median survival time to that of WT-infected mice. Organ burdens were also determined in WT- and *pho81Δ+PHO81*-infected mice at time-of-death and in *pho81Δ*-infected mice at 60 days postinfection. Similar to what was observed for the 5-PP-IP₅-binding defective strain, the lung and brain burdens were reduced substantially in *pho81Δ*-infected mice relative to both WT- and *pho81Δ+PHO81*-infected mice (Fig. 8E and F), consistent with the inability of this strain to establish a lung infection and disseminate to the brain.

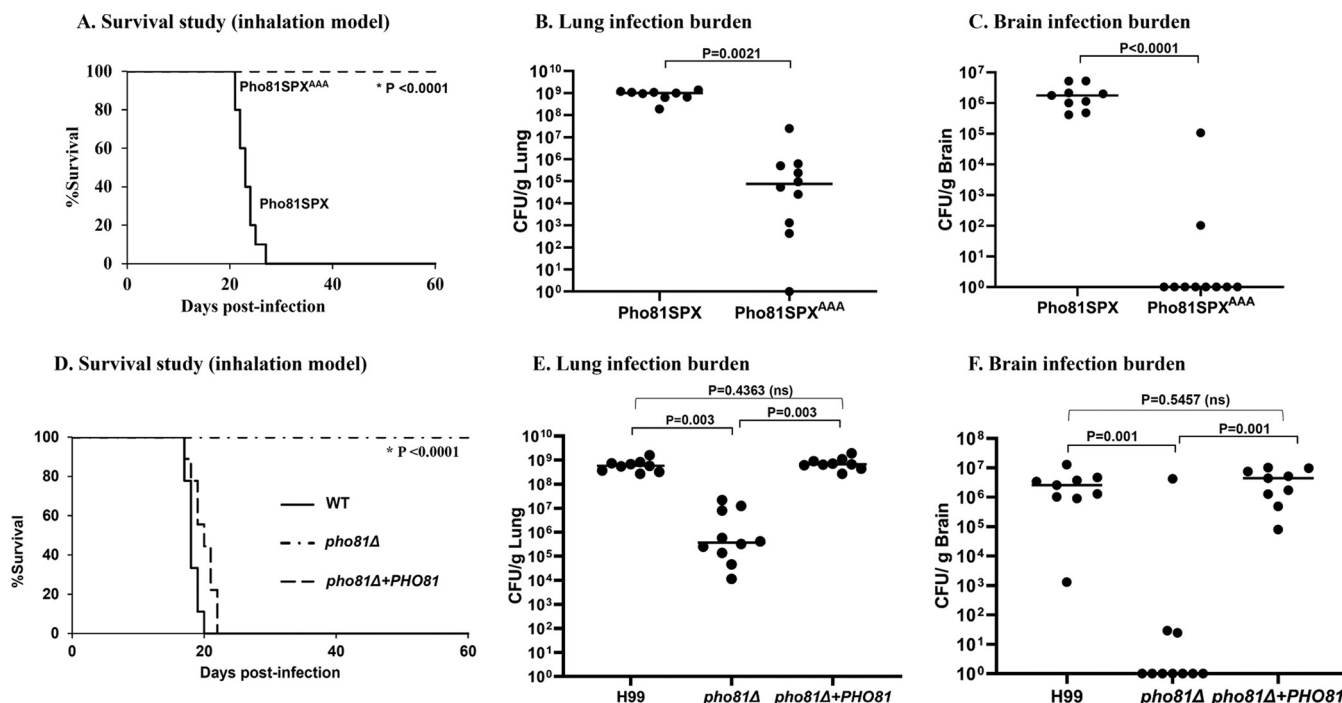


FIG 8 5-PP-IP₅-Pho81 interaction is critical for fungal virulence and dissemination in a mouse infection model. Mice were infected intranasally with 2×10^5 Pho81SPX or Pho81SPX^{AAA} cells (A) or WT, *pho81Δ*, or *pho81Δ+PHO81* cells (D), and their health was monitored for up to 60 days. Infection burdens in the lung (B and E) and brain (C and F) were determined at time of death (Pho81SPX-, WT-, and *pho81Δ+PHO81*-infected mice) and at 60 days postinfection (Pho81SPX^{AAA} and *pho81Δ*-infected mice). Lungs and brains were homogenized, serially diluted, and plated onto agar plates. Plates were incubated at 30°C for 2 days. Colony counts were adjusted to reflect CFU per gram of tissue. The difference in survival (log-rank test) and organ burden (Mann-Whitney U test/two-paired t test) between Pho81SPX- or Pho81SPX^{AAA}-infected groups is statistically significant (i.e., $P \leq 0.0021$ in all cases). No difference in survival and organ burden was observed between the WT and *pho81Δ+PHO81* infection groups. However, the reductions in survival and organ burden observed for the *pho81Δ*-infected mice, relative to the two control strains, was statistically significant (i.e., $P \leq 0.003$ in all cases).

DISCUSSION

Our work has shown that the inositol polyphosphate biosynthesis pathway in *C. neoformans* intersects with the PHO pathway signaling machinery via Kcs1-derived 5-PP-IP₅ rather than via Asp1/Vip1-derived 1-PP-IP₅, providing evidence of evolutionary rewiring with respect to inositol pyrophosphate regulation of the PHO pathway. We also show that 5-PP-IP₅ exerts much of its effect on virulence by promoting PHO pathway activation via its interaction with the SPX domain of Pho81.

Using crystallographic, biochemical, and genetic analysis, Wild et al. demonstrated that recombinant SPX domains from yeast, filamentous fungal, plant, and human proteins bind 5-PP-IP₅, IP₆, and IP₈ with high affinity but not IP₃/IP₄/IP₅ or free orthophosphate. These researchers also identified conserved lysine residues responsible for PP-IP binding. Substituting these lysine residues with alanine did not impact secondary or tertiary structure of SPX domains but did abrogate PP-IP binding (16). By adopting the same approach and incorporating the same alteration into the SPX domain of the full-length protein, we now extend these findings to Pho81 in *C. neoformans*, demonstrating that mutation of the conserved lysine residues prevents Pho81 from binding to 5-PP-IP₅.

From our investigation of CDK component association by 1D-LC-MS and Western blotting, we propose a model where Pho81 association with Pho85-Pho80 depends on 5-PP-IP₅ interaction with the Pho81 SPX domain and where 5-PP-IP₅-Pho81 interaction promotes PHO pathway activation (Fig. 6). 5-PP-IP₅ therefore has a bridging role by promoting the association of CDK complex components, irrespective of phosphate status. Although phosphate deprivation coincided with a decline in 5-PP-IP₅ levels, more CDK complex formation was observed (Fig. 5, lane 3), suggesting that the levels of 5-PP-IP₅ under these conditions were sufficient to promote increased CDK complex

formation. Interestingly, we found that mutant Pho81 became unstable during P_i deprivation (Fig. 5A, lane 4). This could be attributable to 5-PP-IP₅ stabilizing Pho81, in addition to stabilizing the association of Pho81 with the cyclin-dependent kinase complex. The reason why mutant Pho81 instability was not as obvious in the presence of P_i (Fig. 5A, lane 2) could be due to residual binding of 5-PP-IP₅ and higher 5-PP-IP₅ availability. In support of this, we were unable to detect WT Pho81 in a 5-PP-IP₅-deficient background.

Our model in Fig. 6 also supports a role for 5-PP-IP₅-Pho81 interaction in stabilizing the association of Pho81 with Pcl6/7-Pho85 to fine-tune glycogen metabolism. Although *PCL6/7* is a phosphate-responsive gene, we showed that it is dispensable for PHO pathway activation. In *S. cerevisiae*, Pho85 interacts with 10 cyclins, including Pho80, Plc6, and Pcl7, to regulate the PHO pathway, cell cycle, polarity, and glycogen metabolism (42–45). In addition to Pho80 and Pcl6/7, *C. neoformans* has five other cyclins. However, since we did not detect their association with Pho81, they are unlikely to direct phosphate-dependent activity of Pho85.

In support of our data showing that 5-PP-IP₅ functions as an intermolecular stabilizer, there are other examples of where IP and PP-IP interactions with SPX and non-SPX domains stabilize multiprotein complexes. In a model plant *Arabidopsis thaliana*, 1,5-PP-IP₅ (IP₈) facilitates interaction of SPX1 with the PHR1 transcriptional regulator of the phosphate starvation response when phosphate is present (17). This response is triggered by a drop in the abundance of IP₈ upon phosphate deprivation. In mammalian cells, IP₄ stabilizes the histone deacetylase HDAC3-SMRT corepressor complex via non-SPX domain interactions to regulate gene expression. In this context, IP₄ acts as “intermolecular glue” by wedging into a positively charged pocket formed at the interface between the two proteins (46–48).

Wild et al. (16) proposed that inositol polyphosphates communicate cytosolic phosphate levels to SPX domains to regulate phosphate uptake, transport, and storage in fungi, plants, and animals. However, our findings indicate that although 5-PP-IP₅ interaction with the Pho81 SPX domain is essential for PHO pathway activation in *C. neoformans*, PHO pathway activation is not triggered by 5-PP-IP₅ but rather by additional signaling component(s). The following evidence supports this conclusion: several reports, including this study, show that the intracellular concentration of inositol pyrophosphates, including 5-PP-IP₅, decreases during phosphate starvation (16, 17, 36). The decreased abundance of 5-PP-IP₅ is unlikely to trigger PHO pathway activation as the pathway is constitutively repressed in the 5-PP-IP₅-deficient *kcs1Δ* mutant. Furthermore, Pho81-Pho85-Pho80/5-PP-IP₅ complexes are present even when phosphate is available, and their abundance increases upon phosphate deprivation. It is likely that 5-PP-IP₅ molecules wedged inside the complexes are partially protected from degradation and therefore have a slower turnover than free 5-PP-IP₅. Taken together, our data suggest that preformed CKI-CDK/5-PP-IP₅ complexes await signals other than fluctuating 5-PP-IP₅ levels to trigger a phosphate starvation response.

Crystallographic, biochemical, and genetic analysis are required to map regions in cryptococcal Pho80 that interact with Pho81 and potentially with 5-PP-IP₅. In *S. cerevisiae*, two sites on Pho80 involved in binding Pho4 and Pho81 were identified that are markedly distant to each other and the active site (45). These regions will serve as a guide to map the corresponding regions in cryptococcal Pho80. Pho81 in *S. cerevisiae* was also shown to inhibit Pho80-Pho85 via a novel 80-residue motif adjacent to the ankyrin repeats (called the minimal domain [MD]). This MD was shown to be necessary and sufficient for Pho81 function as a Pho85 inhibitor. This is in contrast to mammalian CKIs, which exert their regulatory function via ankyrin repeats. Domain mapping and structural studies will allow assessment of whether an MD exists in cryptococcal Pho81 to provide a second point of contact between 5-PP-IP₅-Pho81 and cyclins.

SPX domains have been reported to undergo a conformational change upon ligand binding (16). Structural comparison of 5-PP-IP₅-bound and free cryptococcal Pho81 may therefore shed light on whether 5-PP-IP₅ binding induces a conformational change in Pho81. Complementary data can be obtained by creating Pho81 deletion variants to

map regions required for binding 5-PP-IP₅ and cyclins. This information will promote understanding of how conformational changes triggered by 5-PP-IP₅ binding affect Pho81 association with Pho80-Pho85 to bring about CDK inhibition and PHO pathway activation. It will also address why the outcome of 5-PP-IP₅-SPX domain interaction leads to different responses in different yeast species and provide insight into the physiological relevance of specific IP species in PHO pathway function.

We previously demonstrated that deletion of the cryptococcal gene encoding the transcription factor, Pho4, led to constitutive repression of the PHO pathway regardless of phosphate status, reduced growth at alkaline pH, a condition that mimics phosphate starvation and hypovirulence in a mouse inhalation model. The loss of virulence in the *pho4Δ* mutant was characterized by a higher median survival time of *pho4Δ*-infected mice relative to WT-infected mice, reduced lung colonization, and the almost complete prevention of fungal dissemination to the host brain (3). In this study, we found that growth of the Pho81-SPX^{AAA} strain was also inhibited at alkaline pH. However, Pho81-SPX^{AAA} virulence was reduced even more substantially: in contrast to infection with the *pho4Δ* mutant where only 50% of the mice succumbed to infection, all mice infected with the Pho81-SPX^{AAA} strain survived and infection burdens in lung and brain were drastically reduced. The infection kinetics and organ burdens observed for Pho81-SPX^{AAA}-infected mice were similar to those observed for *pho81Δ*-infected mice, suggesting that Pho81 promotes invasive fungal disease predominantly via its association with PP-IP₅. A potential explanation for why the Pho81 mutants are more attenuated in virulence than the *pho4Δ* mutant is that 5-PP-IP₅-bound Pho81 regulates more than one CDK complex (see model in Fig. 6). 5-PP-IP₅ may therefore regulate cellular functions other than phosphate homeostasis, namely, glycogen metabolism. Alternatively, Pho81 may have PP-IP₅-dependent cellular function involving interactions with proteins other than CDK components.

In summary, we provide additional evidence of evolutionary divergence in PHO pathway regulation in a fungal pathogen of medical significance by demonstrating that interaction of the IP₇ isomer 5-PP-IP₅, not 1-PP-IP₅, with the Pho81 SPX domain is essential for PHO pathway activation. The critical roles of 5-PP-IP₅ and Pho81 in fungal virulence are conveyed primarily via the interaction of 5-PP-IP₅ with the Pho81 SPX domain. Finally, we demonstrate that 5-PP-IP₅ functions as intermolecular “glue” to stabilize Pho81 association with Pho85/Pho80, providing novel mechanistic insight into how inositol pyrophosphates regulate the PHO pathway. Since Pho81 has no homologue in mammalian cells, disrupting fungal Pho81 function is a potential antifungal strategy.

MATERIALS AND METHODS

Fungal strains and growth conditions. Wild-type *C. neoformans* var. *grubii* strain H99 (serotype A, MAT α) and *S. cerevisiae* WT strain BY4741 were used in this study. All mutant and fluorescent strains created or procured in this study are listed in Table 1 and details of their construction are provided in Materials and Methods and in the supplemental material. Routinely, fungal strains were grown in YPD (1% yeast extract, 2% peptone, and 2% dextrose). Phosphate-deficient minimal medium MM-KCl (29 mM KCl, 15 mM glucose, 10 mM MgSO₄·7H₂O, 13 mM glycine, 3.0 μ M thiamine) was used to induce acid phosphatase activity. KCl was substituted with 29 mM β -glycerol phosphate for drop dilution assay media or 29 mM KH₂PO₄ for MM-KH₂PO₄. The latter was used as a control medium in which acid phosphatase activity was suppressed. In some of the experiments, the cells were grown in phosphate-depleted (low-phosphate) YPD (LP-YPD) to induce PHO pathway activation. LP-YPD was prepared as follows: 5 g yeast extract, 10 g peptone, and 1.23 g MgSO₄ were dissolved in 475 ml of water with prolonged stirring (at least 15 min). Then, 4 ml of concentrated NH₄OH was added dropwise, while the medium was vigorously stirred. The salts were allowed to precipitate for at least 30 min at room temperature. The medium was filtered through a 45- μ m filter, supplemented with 10 g dextrose, and adjusted to pH ~6.5 with concentrated HCl. The resulting medium was filter sterilized.

Mice. The Australian Resource Centre (Western Australia) provided mice (C57BL/6) for the virulence experiments. The mice weighed between 20 and 22 g (6 to 8 weeks old), and the sex was female. Maintenance and care conditions were as follows. Access to food (autoclavable rat and mouse chow supplied by Specialty Feeds) and water was unrestricted, and the light-dark cycle was 12 h. Before experiments, the acclimatization period for the animals was 1 week. Animal experiments were performed in accordance with protocol 4254.03.16, approved by the Western Sydney Local Health District animal ethics committee.

Virulence studies in mice. Female C57BL/6 mice (10 per infection group) were anesthetized by inhalation of 3% isoflurane in oxygen and infected with 2×10^5 fungal cells via the nasal passages as described previously (4). Mice were monitored daily and euthanized by CO₂ asphyxiation when they had lost 20% of their preinfection weight or prior if showing debilitating symptoms of infection, i.e., loss of appetite, moribund appearance, or labored breathing. Median survival differences were estimated using a Kaplan-Meier method. Post euthanasia, the lungs and brain were removed, weighed, and mechanically disrupted in 2 ml of sterile PBS using a BeadBug (Benchmark Scientific). Organ homogenates were serially diluted and plated onto Sabouraud dextrose agar plates. Plates were incubated at 30°C for 2 days. Colony counts were performed and adjusted to reflect the total number of CFU per gram of tissue.

Strain creation. (i) Pho81 SPX mutant with or without GFP tag. Lysine residues in the Pho81 SPX domain putatively involved in binding 5-PP-IP₅ (K^{221,223,228}) were identified by sequence alignment. The Pho81 SPX mutant strain (Pho81SPX^{AAA}) and its control strain (Pho81SPX) were then created in a multistep process (see Fig. S3). First, the SPX domain of *PHO81* was deleted in the WT H99 strain. Second, genomic DNA encoding the 5' end of *PHO81*, including the SPX domain, was amplified to generate native and mutated versions. In the mutated version, codons encoding lysine 221, 223, and 228 were exchanged for those encoding alanine by overlap PCR. Native (NAT) and mutant (AAA) fragments were then fused to the *GDE2* promoter (*GDE2p*) and a dominant resistance marker by overlap PCR and used to reconstitute the *spxD* genotype by homologous recombination. The *GDE2* promoter (*GDE2p*) was used to replace the native *GDE1* promoter of Pho81, because Pho81 shares its promoter with the adjacent gene, *CNAG_02542*. *GDE2p* was a suitable choice because *PHO81/GDE1* and *GDE2* are induced to a similar extent by Pho4 during phosphate deprivation (3). In a third step, WT and mutant *PHO81* were tagged with GFP at the C terminus. The KUTAP vector containing GFP optimized for fluorescence in *C. neoformans* was a gift from Peter Williamson (NIAID, NIH, Bethesda, MD). Each step, including the dominant resistance markers used, is described in more detail below and is summarized in Fig. S3A.

Step 1: deletion of the *PHO81* SPX domain. To delete the *PHO81* SPX domain (see Fig. S3A, step 1), the SPX deletion construct was created by overlap PCR, joining the 5' flank, the hygromycin resistance cassette with the *ACT1* promoter and *GAL7* terminator (Hyg^r), and the 3' flank. The 5' flank, consisting of 977 bp upstream of the *PHO81* gene, was PCR amplified from genomic DNA using the primers PHO81_ots_s and (HygB)PHO81-5'a. The 3' flank, consisting of 1,275 bp downstream of the SPX domain, was PCR amplified using the primers (HygB)PHO81-3's and PHO81_ots_3'a. Hyg^r was PCR amplified with the primers Neo-s and HygB_a (49). The three fragments were fused together using the primers PHO81_5's and PHO81_3'flank-a, and the resulting 4,955-bp product was used to delete the SPX domain from *PHO81* in the H99 WT strain, using biolistic transformation (50). Hygromycin B-resistant (Hyg^r) colonies were screened by PCR amplification across the SPX external recombination junctions using the primers indicated in Table S1 in the supplemental material. A successful transformant was used in step 2 to create the Pho81SPX and Pho81SPX^{AAA} strains.

Step 2: reconstitution of *spxD* with SPX (Pho81SPX) or SPX^{AAA} (Pho81SPX^{AAA}). For the reconstitution of *spxD* with SPX (Pho81SPX) or SPX^{AAA} (Pho81SPX^{AAA}) (see Fig. S3A, step 2), the following three fragments were fused together by overlap PCR: (i) the neomycin resistance cassette with *ACT1* promoter and *TRP1* terminator (Neo^r), (ii) the *GDE2p* to drive expression of *PHO81*, and (iii) the *PHO81* gene sequence consisting of the 1,070-bp SPX domain (native or AAA) and 1,275 bp downstream of SPX. Neo^r was PCR amplified from pJAF1 using the primer pair Neo-s and Neo-a. H99-derived *GDE2p* was PCR amplified using the primer pair (NEO)GDE2p-s and (SPX)GDE2p-a. The 2,345-bp native *PHO81* SPX fragment (SPX^{Nat}) was PCR amplified using the primer pair SPX-start-s and PHO81_ots_3'a. The mutant *PHO81* SPX fragment (SPX^{AAA}) was created by PCR amplifying the 1,070-bp SPX domain and 1,275 bp downstream of SPX using the primer pairs SPX-start-s/Pho81-AAA-a and Pho81-AAA-s/PHO81_ots_3'a, which introduced the mutation at the adjoining ends. The two fragments were then fused together by overlap PCR, using the primer pairs SPX-start-s and PHO81_ots_3'a, to introduce the A^{221,223,228} mutations in the overlapping region. A third PCR was then used to fuse Neo^r-*GDE2p*-SPX^{Nat} or Neo^r-*GDE2p*-SPX^{AAA} using the primer pair Neo-s and PHO81_3'flank-a. The final products were introduced into the Δ *spX* strain created in step 1, resulting in strains Pho81SPX^{Nat} and Pho81SPX^{AAA}. Geneticin-resistant, hygromycin-sensitive transformants were screened by PCR amplification across the Neo^r-*GDE2p*-SPX recombination junctions (see Fig. S3B) using the primers indicated in Table S1.

Step 3: GFP-tagging Pho81SPX and Pho81SPX^{AAA}. For GFP-tagging Pho81SPX and Pho81SPX^{AAA} (see Fig. S1B, step 3), a construct consisting of (i) the 5' flank, encoding 865 bp of the 3' end of the *PHO81* gene without the stop codon; (ii) GFP fused to the nourseothricin resistance cassette (Nat^r); and (iii) the 3' flank, encoding 866 bp downstream of the *PHO81* gene, was created by overlap PCR. The 5' flank was PCR amplified from H99 genomic DNA using the primer pair Pho81-ots-s and Pho81-3f-a (GFP). Using the primers GFP-start-s and Neo-a, GFP-Nat^r (3,116 bp) was PCR amplified from the pCR21 vector (Invitrogen) into which GFP-Nat^r had previously been cloned. The 3' flank was PCR amplified from genomic DNA using the primer pair Pho81-3f-s_(NEO) and Pho81-ots-a. These three overlapping fragments were fused by a final overlap PCR using the primer pair Pho81-5f-s and Pho81-3f-a. The final product was introduced into strains *Pho81SPX* and *Pho81SPX^{AAA}*, creating *GDE2p*-Pho81-GFP and *GDE2p*-Pho81^{AAA}-GFP, respectively, using biolistic transformation. Nourseothricin-resistant transformants were screened by PCR amplifying regions across recombination junctions (see Fig. S3B) using the primers described in Table S1.

(ii) PHO81 deletion and rescue. A *PHO81* gene deletion construct was created by joining the 5' flank (963 bp of genomic DNA upstream of the *PHO81* coding sequence), the hygromycin B resistance (Hyg^r) cassette (with the *ACT1* promoter and *GAL7* terminator), and the 3' flank (1,424 bp of genomic DNA downstream of the *PHO81* coding sequence). The three fragments were fused by overlap PCR using the primer pair PHO81_5's and PHO81_3'a. This deletion construct was used to transform the H99 WT

strain using biolistics (50), creating $\Delta pho81:HYGB$. Hygromycin-resistant colonies were screened by PCR amplification across the 5' and 3' recombination junctions using the primers indicated in Fig. S4 and Table S1 to confirm that homologous recombination had occurred at the correct site.

To create the *PHO81* reconstituted strain ($\Delta pho81+PHO81$), the genomic *PHO81* locus, which comprised the coding region and 5,727 bp upstream and 345 bp downstream of the coding region, was PCR amplified from genomic DNA prepared from the H99 WT strain using the primer pair PHO81_5's and (NEO)PHO81-Rec-5'a. The neomycin resistance (Neo^r) cassette (with the *ACT1* promoter and *TRP1* terminator) was PCR amplified from pJAF (51) using the primer pair Neo-s and Neo-a. The two fragments were fused by overlap PCR using the primer pair PHO81-Rec-5's and Neo-a, and the resulting gene fusion was used to transform the $\Delta pho81$ mutant using biolistics as described above. Neomycin-resistant transformants were screened for their ability to secrete acid phosphatase (Aph1) using the colorimetric pNPP reporter assay described previously (3). This phenotype was lost following deletion of *PHO81* in the WT strain. Transformants that tested positive for secreted acid phosphatase activity were tested further for the presence of the *PHO81* gene by PCR amplifying an internal region of the *PHO81* locus from genomic DNA using the primers indicated in Fig. S4 and Table S1.

(iii) PHO85-mCherry strain. To create a WT *C. neoformans* strain expressing *PHO85* as an mCherry fusion protein, a construct consisting of (i) the 5' flank, 1,141 bp of 3' end of the *PHO85* gene without the stop codon; (ii) mCherry; (iii) the hygromycin resistance cassette (Hyg^r) with the *ACT1* promoter and *GAL7* terminator; and (iv) the 3' flank, 988 bp downstream of the *PHO85* gene, was created by overlap PCR. The 5' flank was PCR amplified from H99 WT genomic DNA using the primer pair PHO85-int-s1 and (mCherry)PHO85-a. The mCherry was PCR amplified from pNEO-mCherry vector using the primer pair (PHO85)mCherry-s and (ActP)-mCherry-a. Hyg^r was generated using the primer pair Neo-s and HygB-a. The 3' flank was PCR amplified from H99 WT genomic DNA using the primer pair (Gal7t)PHO85-3'flank-s and PHO85-3'flank-a1. These four fragments were fused by overlap PCR using the primer pair PHO85-int-s3 and PHO85-3'flank-a3, and the final product was then used to transform H99 WT using biolistic transformation (50). Hygromycin-resistant colonies were screened by PCR amplification across the recombination junctions using primers listed in Table S1.

(iv) Pho81SPX-GFP in a WT and *kcs1Δ* background. A DNA construct consisting of (i) the 5' flank, encoding 865 bp of the 3' end of the *PHO81* coding region minus the stop codon, (ii) GFP fused to the nourseothricin resistance cassette (Nat^r), and (iii) the 3' flank, encoding 866 bp downstream of the *PHO81* coding region, was amplified by PCR from genomic DNA prepared from the Pho81SPX-GFP strain used in Fig. 5 using the primer pair Pho81-5f-s and Pho81-3f-a. The final 4,559-bp product was introduced into the *kcs1Δ:NEO* strain (4) using biolistic transformation. Nourseothricin-resistant transformants were screened by PCR by amplifying regions across the recombination junctions using the primers described in Table S1.

Assessing PHO pathway activation. (i) Acid phosphatase reporter assay. Extracellular acid phosphatase (APase) activity associated with the *APH1* gene product was measured as previously described (5). Briefly, YPD overnight cultures were centrifuged, and the pellets were washed twice with water and resuspended in PHO pathway-inducing and noninducing medium (see above) at an optical density at 600 nm (OD₆₀₀) of 1. The cultures were incubated at 30°C for 3 h or as indicated otherwise. After incubation, 200 μ l of each culture was centrifuged, and the pellets were resuspended in 400 μ l of APase reaction mixture (50 mM sodium acetate [pH 5.2], 2.5 mM *p*-nitrophenyl phosphate [pNPP]). Reactions were performed at 37°C for 5 to 15 min, which was the time determined to be within the linear range of APase activity (5). Reactions were stopped by adding of 800 μ l of 1 M Na₂CO₃. APase-mediated hydrolysis of pNPP was quantified spectrophotometrically at 420 nm. Any growth difference among strains was corrected by measuring the OD₆₀₀ prior to performing the assay, and the APase activity was calculated as OD₄₂₀/OD₆₀₀. In some cases, the APase activity was normalized to the WT and expressed as a fold change. In the experiment where PHO pathway activation in the absence of phosphate was measured over a 2-day time course, 10 to 300 μ l of culture was used for the APase activity assay, with smaller amounts needed at longer induction times to prevent reaction saturation due to increased culture growth. All assays were performed in biological triplicate.

(ii) Quantitative PCR. RNA extraction, cDNA synthesis, and qPCR of PHO genes in *C. neoformans* strains was performed as described previously (3). The sequences of primers used for qPCR are listed in Table S1.

Fractionating ³H-labeled inositol polyphosphates. [³H]inositol labeling of fungal cells was performed as previously described (52), with modifications (4). Overnight fungal cultures grown in YPD were diluted to an OD₆₀₀ of 0.05 in fresh YPD containing 10 mCi/ml [³H]myo-inositol (Perkin-Elmer) and incubated until an OD₆₀₀ of >6. The cells were pelleted, washed, and resuspended in MM with or without phosphate (as indicated). After an additional 2 h of incubation, fungal cells were pelleted, washed, and snap-frozen in liquid nitrogen. To extract inositol polyphosphates, the cells were resuspended in extraction buffer (1 M HClO₄, 3 mM EDTA, 0.1 mg/ml IP₆) and homogenized with glass beads using a bead beater. Debris was pelleted, and the supernatants were neutralized (1 M K₂CO₃, 3 mM EDTA) and stored at 4°C. The radiolabeled inositol polyphosphates were fractionated by anion-exchange high-pressure liquid chromatography (HPLC).

Creation of a 5-PP-IP₅ affinity capture resin. Synthesis of resin-bound 5PP-IP₅, a diphosphoinositol polyphosphate analog containing a nonhydrolyzable bisphosphonate group in the 5-position as described in detail by Wu et al. (37). This bisphosphonate analog closely resembles the natural molecule, both structurally and biochemically, while exhibiting increased stability toward hydrolysis in a cell lysate (53).

Assessing binding of Pho81 to 5-PP-IP₅. GFP-labeled strains were grown for 5 h in LP-YPD (P_i-culture) or overnight in YPD (P_i+ culture). The cells were pelleted by centrifugation, and lysates were prepared as described above using lysis buffer (50 mM Tris [pH 7.5], 150 mM NaCl, 0.05% Triton X-100, 1 mM EDTA, 1 mM phenylmethylsulfonyl fluoride [PMSF], 1 μl/10 mg cell pellet fungal protease inhibitor cocktail [Sigma, catalog no. P8215]). Protein in each lysate was adjusted to ~8 mg/ml to correct for growth differences and incubated with 5-PCP-IP₅-conjugated resin or phosphate (P_i)-conjugated resin as a control (~200 μl of slurry) (37). Incubation was allowed for 2 h at 4°C. The resin was pelleted by centrifugation, and the supernatant was removed. The resin was then washed three times with lysis buffer. Resin-bound proteins were eluted by resuspension in SDS-PAGE loading buffer and resolved by SDS-PAGE. GFP-tagged proteins were detected by Western blotting with anti-GFP antibody (Santa Cruz Biotechnology, catalog no. sc-9996).

Immunocapture of fluorescent Pho81. Cells were grown overnight in YPD or LP-YPD as indicated. Cell pellets were collected and snap-frozen. At least 120 and 350 mg of cell pellet was used for immunoprecipitation/Western blotting and immunoprecipitation/1D-LC-MS, respectively. Cell pellets were resuspended in 2 volumes of lysis buffer (0.1% NP-40, 250 mM NaCl, 50 mM sodium fluoride, 5 mM EDTA, 50 mM Tris-HCl [pH 7.5], 1 mM DTT, 1 mM PMSF, 1 μl/10 mg cell pellet fungal protease inhibitor cocktail [Sigma, catalog no. P8215]). Lysates were prepared by bead beating the cells in the presence of glass beads (425 to 600 μm), followed by centrifugation at 4°C at maximum speed. GFP-Trap agarose (Chromotek gta-20) was used to immunoprecipitate GFP-tagged Pho81. Protein G-Sepharose 4 Fast Flow (GE Healthcare, catalog no. 17061801) and anti-mCherry antibody (ab-167453; Abcam) were used to immunoprecipitate Pho85-mCherry. Sepharose beads were washed three times in lysis buffer and incubated with the lysate for 2 to 3 h at 4°C. After lysate incubation, the Sepharose was washed three times with lysis buffer and resuspended in SDS-PAGE loading buffer, and the solubilized proteins were resolved by SDS-PAGE. Cell lysates were run as a loading control.

(i) Western blotting. GFP-tagged proteins were detected using anti-GFP antibody (Santa Cruz Biotechnology, sc-9996) and Pho85 was detected using anti PSTAIRE (1:200 dilution; Santa Cruz Biotechnology, sc-53) or anti-PSTAIR antibody (1:200 dilution; Merck, catalog no. 06-923), followed by Amersham ECL anti-rabbit IgG, HRP-linked F(ab')₂ fragment (from donkey; 1:8,000 dilution). Anti-PSTAIR antibodies also detect cryptococcal Cdc2 (Cdc28 in *S. cerevisiae*) in total cell lysates since both Cdc2 and Pho85 contain PSTAIRE motif. Cdc2 was therefore used as a control for protein loading (54). Similar levels of Cdc2 (the main cyclin-dependent kinase in yeast) were detected in whole lysates, confirming that each immunoprecipitation had been performed from lysates containing similar levels of total protein.

(ii) 1D-LC-MS. SDS gels were stained using a colloidal blue staining kit (LC6025; Life Technologies) according to the manufacturer's protocol.

Each lane was cut into five equal pieces and the proteins within each piece were trypsin treated and analyzed by mass spectrometry. Briefly, the gel slices were diced up and destained in a 60:40 solution of 40 mM NH₄HCO₃ (pH 7.8)–100% acetonitrile for 1 h. Gel pieces were vacuum-dried and then rehydrated with a 12-ng/μl trypsin (Promega) solution at 4°C for 1 h. Excess trypsin was removed, and gel pieces were covered with 40 mM NH₄HCO₃ and then incubated overnight at 37°C. Peptides were concentrated and desalted using C18 Zip-Tips (Millipore, Bedford, MA) according to the manufacturer's instructions. Peptides were resuspended in 10 μl of 3% (vol/vol) acetonitrile–0.1% (vol/vol) formic acid and briefly sonicated. Samples were separated by nano-LC using an Ultimate 3000 HPLC and autosampler system (Thermo Fisher Scientific, Scoresby, UK) coupled to an in-house fritless nano-LC 75 μm × 40 cm column packed with ReproSil Pur 120 C₁₈ in the stationary phase (1.9 μm, Dr. Maisch GmbH, Ammerbuch, Germany). LC mobile phase buffers were comprised of solvent A (0.1% [vol/vol] formic acid) and solvent B (80% [vol/vol] acetonitrile, 0.1% [vol/vol] formic acid). Peptides were eluted using a linear gradient of 5% B to 35% B over 60 min, followed by a 95% B wash over 1 min at a flow rate of 250 nl/min. The LC was coupled to a Q Exactive Plus Orbitrap mass spectrometer (Thermo Fisher Scientific). The column voltage was 2,300 V, and the heated capillary was set to 275°C. Positive ions were generated by electrospray, and the Orbitrap was operated in data-dependent acquisition mode. A survey scan of 350 to 1,550 *m/z* was acquired (resolution = 35,000, with an accumulation target value of 3,000,000 ions) with lockmass enabled. Up to 20 of the most abundant ions (>1.7E5 ions), with charge states of ≥+2 and <+6, were sequentially isolated and fragmented, and a target value of 100,000 ions were collected. Ions selected for tandem mass spectrometry (MS/MS) were dynamically excluded for 20 s. The data were analyzed using Proteome Discoverer v2.3 (Thermo Fisher Scientific) and Mascot v2.4 (Matrix Science, London, UK). The search parameters included the following variable modifications: oxidized methionine, acetyl (protein N-term), deamidated asparagine/glutamine, and carbamidomethyl cysteine. The enzyme was set to trypsin, and the precursor mass tolerance was set to 10 ppm, while the fragment tolerance was 0.05 Da. The databases were the *C. neoformans* H99 from FungiDB v44 (fungidb.org) and a common contaminants database. Proteins were quantified by using the minora feature detector node and precursor ion quantifier node.

Statistics. Statistical analysis for virulence studies was performed using SPSS (SPSS, Chicago, IL), SAS Studio (SAS Institute, Inc.), and Prism (v8.0; GraphPad Software, Inc., San Diego, CA) statistical software. Differences in mouse mortality were determined by comparing survival curves of different infected groups using a log-rank test. Differences in CFU were assessed by using a two-sample *t* test or a Mann-Whitney U test when data were not normally distributed. One-way analysis of variance (ANOVA) or a Student *t* test was used in all other experiments, as indicated in the figure legends. All plotted data represent means ± the standard deviations. Results were considered significant at a *P* value of <0.05.

SUPPLEMENTAL MATERIAL

Supplemental material is available online only.

TABLE S1, PDF file, 0.1 MB.

FIG S1, PDF file, 0.02 MB.

FIG S2, PDF file, 0.04 MB.

FIG S3, PDF file, 0.3 MB.

FIG S4, PDF file, 0.1 MB.

FIG S5, PDF file, 0.01 MB.

FIG S6, PDF file, 0.1 MB.

FIG S7, PDF file, 0.02 MB.

FIG S8, PDF file, 0.1 MB.

ACKNOWLEDGMENTS

This study was supported by project grants from the National Health and Medical Research Council of Australia (APP1058779 and APP1183939). The funders had no role in study design, data collection, and interpretation or the decision to submit the work for publication. We acknowledge that the *pcl6/7Δ* strain was obtained from the Madhani knockout library (<http://www.fgsc.net/crypto/crypto.htm>), which was created using NIH funding (R01AI100272). S.L. is supported by a Career Development Award from the Westmead Institute for Medical Research. qPCR and fluorescence microscopy were performed at the Westmead Scientific Platforms, which are supported by the Westmead Research Hub, the Cancer Institute New South Wales, the National Health and Medical Research Council and the Ian Potter Foundation. Animal experiments were performed at the Westmead Institute for Medical Research Biological Services Facility.

We thank Bin He (University of Iowa) for helpful discussion regarding PHO regulation in fungi.

REFERENCES

- Rajasingham R, Smith RM, Park BJ, Jarvis JN, Govender NP, Chiller TM, Denning DW, Loyse A, Boulware DR. 2017. Global burden of disease of HIV-associated cryptococcal meningitis: an updated analysis. *Lancet Infect Dis* 17:873–881. [https://doi.org/10.1016/S1473-3099\(17\)30243-8](https://doi.org/10.1016/S1473-3099(17)30243-8).
- Kozubowski L, Lee SC, Heitman J. 2009. Signalling pathways in the pathogenesis of cryptococcus. *Cell Microbiol* 11:370–380. <https://doi.org/10.1111/j.1462-5822.2008.01273.x>.
- Lev S, Kaufman-Francis K, Desmarini D, Juillard PG, Li C, Stifter SA, Feng CG, Sorrell TC, Grau GE, Bahn YS, Djordjevic JT. 2017. Pho4 is essential for dissemination of *Cryptococcus neoformans* to the host brain by promoting phosphate uptake and growth at alkaline pH. *mSphere* 2:e00381-16. <https://doi.org/10.1128/mSphere.00381-16>.
- Lev S, Li C, Desmarini D, Saiardi A, Fewings NL, Schibeci SD, Sharma R, Sorrell TC, Djordjevic JT. 2015. Fungal inositol pyrophosphate IP₇ is crucial for metabolic adaptation to the host environment and pathogenicity. *mBio* 2:e00531-15. <https://doi.org/10.1128/mBio.00531-15>.
- Lev S, Crosssett B, Cha SY, Desmarini D, Li C, Chayakulkeeree M, Wilson CF, Williamson PR, Sorrell TC, Djordjevic JT. 2014. Identification of Aph1, a phosphate-regulated, secreted, and vacuolar acid phosphatase in *Cryptococcus neoformans*. *mBio* 5:e01649-14–e01614. <https://doi.org/10.1128/mBio.01649-14>.
- Li C, Lev S, Desmarini D, Kaufman-Francis K, Saiardi A, Silva APG, Mackay JP, Thompson PE, Sorrell TC, Djordjevic JT. 2017. IP₃-4 kinase Arg1 regulates cell wall homeostasis and surface architecture to promote clearance of *Cryptococcus neoformans* infection in a mouse model. *Virulence* 8:1833–1848. <https://doi.org/10.1080/21505594.2017.1385692>.
- Li C, Lev S, Saiardi A, Desmarini D, Sorrell TC, Djordjevic JT. 2016. Identification of a major IP₅ kinase in *Cryptococcus neoformans* confirms that PP-IP₅/IP₇, not IP₆, is essential for virulence. *Sci Rep* 6:23927. <https://doi.org/10.1038/srep23927>.
- Lev S, Desmarini D, Li C, Chayakulkeeree M, Traven A, Sorrell TC, Djordjevic JT. 2013. Phospholipase C of *Cryptococcus neoformans* regulates homeostasis and virulence by providing inositol trisphosphate as a substrate for Arg1 kinase. *Infect Immun* 81:1245–1255. <https://doi.org/10.1128/IAI.01421-12>.
- Shears SB. 2018. Intimate connections: inositol pyrophosphates at the interface of metabolic regulation and cell signaling. *J Cell Physiol* 233:1897–1912. <https://doi.org/10.1002/jcp.26017>.
- Wilson MS, Livermore TM, Saiardi A. 2013. Inositol pyrophosphates: between signalling and metabolism. *Biochem J* 452:369–379. <https://doi.org/10.1042/BJ20130118>.
- Li J, Zhang B, Ma T, Wang H, Zhang B, Yu Q, Li M. 2017. Role of the inositol polyphosphate multikinase Ipk2 in regulation of hyphal development, calcium signaling and secretion in *Candida albicans*. *Mycopathologia* 182:609–623. <https://doi.org/10.1007/s11046-017-0138-4>.
- Desfougères Y, Gerasimaitė RU, Jessen HJ, Mayer A. 2016. Vtc5, a novel subunit of the vacuolar transporter chaperone complex, regulates polyphosphate synthesis and phosphate homeostasis in yeast. *J Biol Chem* 291:22262–22275. <https://doi.org/10.1074/jbc.M116.746784>.
- Secco D, Wang C, Arpat BA, Wang Z, Poirier Y, Tyerman SD, Wu P, Shou H, Whelan J. 2012. The emerging importance of the SPX domain-containing proteins in phosphate homeostasis. *New Phytol* 193:842–851. <https://doi.org/10.1111/j.1469-8137.2011.04002.x>.
- Secco D, Wang C, Shou H, Whelan J. 2012. Phosphate homeostasis in the yeast *Saccharomyces cerevisiae*, the key role of the SPX domain-containing proteins. *FEBS Lett* 586:289–295. <https://doi.org/10.1016/j.febslet.2012.01.036>.
- Wang C, Huang W, Ying Y, Li S, Secco D, Tyerman S, Whelan J, Shou H. 2012. Functional characterization of the rice SPX-MFS family reveals a key role of OsSPX-MFS1 in controlling phosphate homeostasis in leaves. *New Phytol* 196:139–148. <https://doi.org/10.1111/j.1469-8137.2012.04227.x>.
- Wild R, Gerasimaitė R, Jung JY, Truffault V, Pavlovic I, Schmidt A, Saiardi A, Jessen HJ, Poirier Y, Hothorn M, Mayer A. 2016. Control of eukaryotic phosphate homeostasis by inositol polyphosphate sensor domains. *Science* 352:986–990. <https://doi.org/10.1126/science.aad9858>.
- Dong J, Ma G, Sui L, Wei M, Satheesh V, Zhang R, Ge S, Li J, Zhang TE, Wittwer C, Jessen HJ, Zhang H, An GY, Chao DY, Liu D, Lei M. 2019. Inositol pyrophosphate InsP8 acts as an intracellular phosphate signal in *Arabidopsis*. *Mol Plant* 12:1463–1473. <https://doi.org/10.1016/j.molp.2019.08.002>.
- Puga MI, Mateos I, Charukesi R, Wang Z, Franco-Zorrilla JM, de Lorenzo

- L, Irigoyen ML, Masiero S, Bustos R, Rodriguez J, Leyva A, Rubio V, Sommer H, Paz-Ares J. 2014. SPX1 is a phosphate-dependent inhibitor of phosphate starvation response 1 in *Arabidopsis*. *Proc Natl Acad Sci U S A* 111:14947–14952. <https://doi.org/10.1073/pnas.1404654111>.
19. Wang Z, Ruan W, Shi J, Zhang L, Xiang D, Yang C, Li C, Wu Z, Liu Y, Yu Y, Shou H, Mo X, Mao C, Wu P. 2014. Rice SPX1 and SPX2 inhibit phosphate starvation responses through interacting with PHR2 in a phosphate-dependent manner. *Proc Natl Acad Sci U S A* 111:14953–14958. <https://doi.org/10.1073/pnas.1404680111>.
 20. Wilson MS, Jessen HJ, Saiardi A. 2019. The inositol hexakisphosphate kinases IP6K1 and -2 regulate human cellular phosphate homeostasis, including XPR1-mediated phosphate export. *J Biol Chem* 294:11597–11608. <https://doi.org/10.1074/jbc.RA119.007848>.
 21. Azevedo C, Saiardi A. 2017. Eukaryotic phosphate homeostasis: the inositol pyrophosphate perspective. *Trends Biochem Sci* 42:219–231. <https://doi.org/10.1016/j.tibs.2016.10.008>.
 22. Lev S, Djordjevic JT. 2018. Why is a functional PHO pathway required by fungal pathogens to disseminate within a phosphate-rich host: a paradox explained by alkaline pH-simulated nutrient deprivation and expanded PHO pathway function. *PLoS Pathog* 14:e1007021. <https://doi.org/10.1371/journal.ppat.1007021>.
 23. He BZ, Zhou X, O'Shea EK. 2017. Evolution of reduced co-activator dependence led to target expansion of a starvation response pathway. *Elife* 6:e25157. <https://doi.org/10.7554/eLife.25157>.
 24. Kretschmer M, Reiner E, Hu G, Tam N, Oliveira DL, Caza M, Yeon JH, Kim J, Kastrop CJ, Jung WH, Kronstad JW. 2014. Defects in phosphate acquisition and storage influence virulence of *Cryptococcus neoformans*. *Infect Immun* 82:2697–2712. <https://doi.org/10.1128/IAI.01607-14>.
 25. Toh-e A, Ohkusu M, Li HM, Shimizu K, Takahashi-Nakaguchi A, Gono T, Kawamoto S, Kanesaki Y, Yoshikawa H, Nishizawa M. 2015. Identification of genes involved in the phosphate metabolism in *Cryptococcus neoformans*. *Fungal Genet Biol* 80:19–30. <https://doi.org/10.1016/j.fgb.2015.04.019>.
 26. Kaffman A, Herskowitz I, Tjian R, O'Shea EK. 1994. Phosphorylation of the transcription factor PHO4 by a cyclin-CDK complex, PHO80-PHO85. *Science* 263:1153–1156. <https://doi.org/10.1126/science.8108735>.
 27. O'Neill EM, Kaffman A, Jolly ER, O'Shea EK. 1996. Regulation of PHO4 nuclear localization by the PHO80-PHO85 cyclin-CDK complex. *Science* 271:209–212. <https://doi.org/10.1126/science.271.5246.209>.
 28. Ikeh M, Ahmed Y, Quinn J. 2017. Phosphate acquisition and virulence in human fungal pathogens. *Microorganisms* 5:48. <https://doi.org/10.3390/microorganisms5030048>.
 29. Lee YS, Mulugu S, York JD, O'Shea EK. 2007. Regulation of a cyclin-CDK-CDK inhibitor complex by inositol pyrophosphates. *Science* 316:109–112. <https://doi.org/10.1126/science.1139080>.
 30. Lev S, Rupasinghe T, Desmarini D, Kaufman-Francis K, Sorrell TC, Roessner U, Djordjevic JT. 2019. The PHO signaling pathway directs lipid remodeling in *Cryptococcus neoformans* via DGTS synthase to recycle phosphate during phosphate deficiency. *PLoS One* 14:e0212651. <https://doi.org/10.1371/journal.pone.0212651>.
 31. Riekhof WR, Naik S, Bertrand H, Benning C, Voelker DR. 2014. Phosphate starvation in fungi induces the replacement of phosphatidylcholine with the phosphorus-free betaine lipid diacylglyceryl-*N,N,N*-trimethylhomoserine. *Eukaryot Cell* 13:749–757. <https://doi.org/10.1128/EC.00004-14>.
 32. Auesukaree C, Tochio H, Shirakawa M, Kaneko Y, Harashima S. 2005. Plc1p, Arg82p, and Kcs1p, enzymes involved in inositol pyrophosphate synthesis, are essential for phosphate regulation and polyphosphate accumulation in *Saccharomyces cerevisiae*. *J Biol Chem* 280:25127–25133. <https://doi.org/10.1074/jbc.M414579200>.
 33. Gerasimaite R, Pavlovic I, Capolicchio S, Hofer A, Schmidt A, Jessen HJ, Mayer A. 2017. Inositol pyrophosphate specificity of the SPX-dependent polyphosphate polymerase VTC. *ACS Chem Biol* 12:648–653. <https://doi.org/10.1021/acscmbio.7b00026>.
 34. Zhou Z, Wang Z, Lv Q, Shi J, Zhong Y, Wu P, Mao C. 2015. SPX proteins regulate Pi homeostasis and signaling in different subcellular level. *Plant Signal Behav* 10:e1061163. <https://doi.org/10.1080/15592324.2015.1061163>.
 35. Gray N, Devivaud L, Doerig C, Meijer L. 1999. ATP-site directed inhibitors of cyclin-dependent kinases. *Curr Med Chem* 6:859–875.
 36. Lonetti A, Szigyarto Z, Bosch D, Loss O, Azevedo C, Saiardi A. 2011. Identification of an evolutionarily conserved family of inorganic polyphosphate endopolyphosphatases. *J Biol Chem* 286:31966–31974. <https://doi.org/10.1074/jbc.M111.266320>.
 37. Wu M, Chong LS, Perlman DH, Resnick AC, Fiedler D. 2016. Inositol polyphosphates intersect with signaling and metabolic networks via two distinct mechanisms. *Proc Natl Acad Sci U S A* 113:E6757–E6765. <https://doi.org/10.1073/pnas.1606853113>.
 38. Schneider KR, Smith RL, O'Shea EK. 1994. Phosphate-regulated inactivation of the kinase PHO80-PHO85 by the CDK inhibitor PHO81. *Science* 266:122–126. <https://doi.org/10.1126/science.7939631>.
 39. Huang S, Jeffery DA, Anthony MD, O'Shea EK. 2001. Functional analysis of the cyclin-dependent kinase inhibitor Pho81 identifies a novel inhibitory domain. *Mol Cell Biol* 21:6695–6705. <https://doi.org/10.1128/mcb.21.19.6695-6705.2001>.
 40. Serra-Cardona A, Canadell D, Ariño J. 2015. Coordinate responses to alkaline pH stress in budding yeast. *Microb Cell* 2:182–196. <https://doi.org/10.15698/mic2015.06.205>.
 41. Ikeh MA, Kastora SL, Day AM, Herrero-de-Dios CM, Tarrant E, Waldron KJ, Banks AP, Bain JM, Lydall D, Veal EA, MacCallum DM, Erwig LP, Brown AJ, Quinn J. 2016. Pho4 mediates phosphate acquisition in *Candida albicans* and is vital for stress resistance and metal homeostasis. *Mol Biol Cell* 27:2784–2801. <https://doi.org/10.1091/mbc.E16-05-0266>.
 42. Lee M, O'Regan S, Moreau JL, Johnson AL, Johnston LH, Goding CR. 2000. Regulation of the Pcl7-Pho85 cyclin-cdk complex by Pho81. *Mol Microbiol* 38:411–422. <https://doi.org/10.1046/j.1365-2958.2000.02140.x>.
 43. Wang Z, Wilson WA, Fujino MA, Roach PJ. 2001. The yeast cyclins Pc16p and Pc17p are involved in the control of glycogen storage by the cyclin-dependent protein kinase Pho85p. *FEBS Lett* 506:277–280. [https://doi.org/10.1016/s0014-5793\(01\)02914-3](https://doi.org/10.1016/s0014-5793(01)02914-3).
 44. Tan YS, Morcos PA, Cannon JF. 2003. Pho85 phosphorylates the Glc7 protein phosphatase regulator Glc8 *in vivo*. *J Biol Chem* 278:147–153. <https://doi.org/10.1074/jbc.M208058200>.
 45. Huang K, Ferrin-O'Connell I, Zhang W, Leonard GA, O'Shea EK, Quijcho FA. 2007. Structure of the Pho85-Pho80 CDK-cyclin complex of the phosphate-responsive signal transduction pathway. *Mol Cell* 28:614–623. <https://doi.org/10.1016/j.molcel.2007.09.013>.
 46. Millard CJ, Watson PJ, Celardo J, Gordiyenko Y, Cowley SM, Robinson CV, Fairall L, Schwabe JW. 2013. Class I HDACs share a common mechanism of regulation by inositol phosphates. *Mol Cell* 51:57–67. <https://doi.org/10.1016/j.molcel.2013.05.020>.
 47. Watson PJ, Fairall L, Santos GM, Schwabe JW. 2012. Structure of HDAC3 bound to co-repressor and inositol tetrakisphosphate. *Nature* 481:335–340. <https://doi.org/10.1038/nature10728>.
 48. Watson PJ, Millard CJ, Riley AM, Robertson NS, Wright LC, Godage HY, Cowley SM, Jamieson AG, Potter BV, Schwabe JW. 2016. Insights into the activation mechanism of class I HDAC complexes by inositol phosphates. *Nat Commun* 7:11262. <https://doi.org/10.1038/ncomms11262>.
 49. Hua J, Meyer JD, Lodge JK. 2000. Development of positive selectable markers for the fungal pathogen *Cryptococcus neoformans*. *Clin Diagn Lab Immunol* 7:125–128. <https://doi.org/10.1128/cdli.7.1.125-128.2000>.
 50. Toffaletti DL, Rude TH, Johnston SA, Durack DT, Perfect JR. 1993. Gene transfer in *Cryptococcus neoformans* by use of biolistic delivery of DNA. *J Bacteriol* 175:1405–1411. <https://doi.org/10.1128/jb.175.5.1405-1411.1993>.
 51. Fraser JA, Subaran RL, Nichols CB, Heitman J. 2003. Recapitulation of the sexual cycle of the primary fungal pathogen *Cryptococcus neoformans* var. *gattii*: implications for an outbreak on Vancouver Island, Canada. *Eukaryot Cell* 2:1036–1045. <https://doi.org/10.1128/ec.2.5.1036-1045.2003>.
 52. Azevedo C, Saiardi A. 2006. Extraction and analysis of soluble inositol polyphosphates from yeast. *Nat Protoc* 1:2416–2422. <https://doi.org/10.1038/nprot.2006.337>.
 53. Wu M, Chong LS, Capolicchio S, Jessen HJ, Resnick AC, Fiedler D. 2014. Elucidating diphosphoinositol polyphosphate function with nonhydrolyzable analogues. *Angew Chem Int Ed Engl* 53:7192–7197. <https://doi.org/10.1002/anie.201402905>.
 54. Takeo K, Virtudazo E, Ohkusu M, Kawamoto S, Ito-Kuwa S, Aoki S. 2006. [Cell cycle control and CDC28/Cdc2 homologue and related gene cloning of *Cryptococcus neoformans*]. *Nihon Ishinkin Gakkai Zasshi* 47:257–262. <https://doi.org/10.3314/jjmm.47.257>.
 55. Jung KW, Song DH, Maeng S, Lee KT, So YS, Hong J, Choi J, Byun HJ, Kim H, Bang S, Yang MH, Lee JW, Kim MS, Kim SY, Ji JH, Park G, Kwon H, Cha S, Meyers GL, Wang LL, Jang J, Janbon G, Adedoyin G, Kim T, Averette AK, Heitman J, Cheong E, Lee YH, Lee YW, Bahn YS. 2015. Systematic functional profiling of transcription factor networks in *Cryptococcus neoformans*. *Nat Commun* 6:6757. <https://doi.org/10.1038/ncomms7757>.